

ornl

**OAK RIDGE
NATIONAL
LABORATORY**

MARTIN MARIETTA

MARTIN MARIETTA ENERGY SYSTEMS LIBRARIES



3 4456 0319779 7

ORNL/TM-11381

Shield Design, Analysis, and Testing to Survive Stainless Steel Projectiles

E. D. Brewer
W. R. Hendrich
D. G. Thomas
J. E. Smith

OAK RIDGE NATIONAL LABORATORY

CENTRAL RESEARCH LIBRARY

CIRCULARS SECTION

4500N RD/BN 175

LIBRARY LOAN COPY

DO NOT TRANSFER TO ANOTHER PERSON

If you wish someone else to see this
report, send in name with report and
the library will arrange a loan.

OPERATED BY
MARTIN MARIETTA ENERGY SYSTEMS, INC.
FOR THE UNITED STATES
DEPARTMENT OF ENERGY

This report has been reproduced directly from the best available copy.

Available to DOE and DOE contractors from the Office of Scientific and Technical Information, P.O. Box 62, Oak Ridge, TN 37831; prices available from (615) 576-8401, FTS 826-8401.

Available to the public from the National Technical Information Service, U.S. Department of Commerce, 5285 Port Royal Rd., Springfield, VA 22161.

NTIS price codes—Printed Copy: A05 Microfiche A01

This report was prepared as an account of work sponsored by an agency of the United States Government. Neither the United States Government nor any agency thereof, nor any of their employees, makes any warranty, express or implied, or assumes any legal liability or responsibility for the accuracy, completeness, or usefulness of any information, apparatus, product, or process disclosed, or represents that its use would not infringe privately owned rights. Reference herein to any specific commercial product, process, or service by trade name, trademark, manufacturer, or otherwise, does not necessarily constitute or imply its endorsement, recommendation, or favoring by the United States Government or any agency thereof. The views and opinions of authors expressed herein do not necessarily state or reflect those of the United States Government or any agency thereof.

DEFENSE AND SPACE PROGRAMS

Contribution from
Engineering Technology Division

**SHIELD DESIGN, ANALYSIS, AND TESTING TO SURVIVE
STAINLESS STEEL PROJECTILES**

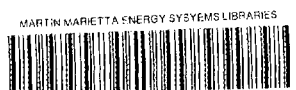
E. D. Brewer
W. R. Hendrich
D. G. Thomas
J. E. Smith

NOTICE This document contains information of a preliminary nature.
It is subject to revision or correction and therefore does not represent a
final report.

DATE PUBLISHED: JANUARY 1990

Prepared for
U.S. Air Force Weapons Laboratory
Kirtland Air Force Base
Albuquerque, New Mexico
under Interagency Agreement DOE No. 40-1663-A1

Prepared by the
OAK RIDGE NATIONAL LABORATORY
Oak Ridge, Tennessee 37831
operated by
MARTIN MARIETTA ENERGY SYSTEMS, INC.
for the
U.S. DEPARTMENT OF ENERGY
under contract DE-AC05-84OR21400



3 4456 0319779 7

TABLE OF CONTENTS

	PAGE
LIST OF TABLES	v
LIST OF FIGURES	vii
ABSTRACT	1
1. INTRODUCTION	1
2. EXPERIMENTAL PROCEDURES	3
3. TEST HARDWARE DESCRIPTION	6
4. TEST RESULTS DESCRIPTION	11
5. TEST RESULTS DISCUSSION	22
6. ANALYSIS METHODS	40
7. ANALYSIS CONFIGURATIONS	43
8. ANALYSIS RESULTS	47
8.1 Comparison of Normal Incidence And Yawed Cylinder Impacts ...	47
8.2 Comparison of Cylindrical and Spherical Projectiles	56
9. COMPARISON OF ANALYTICAL AND TEST RESULTS	64
10. CONCLUSIONS	68
11. RECOMMENDATIONS	70
12. REFERENCES	72

LIST OF TABLES

	<u>Page</u>
Table 1. Hardware summary for stainless steel projectile tests	7
Table 2. Comparison of shield hardware	8
Table 3. Yaw angle at impact for stainless steel projectile tests	12
Table 4. Front plate results	13
Table 5. Summary of back plate results	15
Table 6. Front plate results arranged in order of increasing ellipticity	33
Table 7. Impact velocities/pressures required for projectile melt or vaporization	38
Table 8. Stainless steel analysis summary	44
Table 9. Comparison of analytic and experimental front hole diameters	64

LIST OF FIGURES

Figure 1. Experimental test decision matrix	4
Figure 2. Yaw angle nomenclature	11
Figure 3. Front hole results	13
Figure 4. Disrupter damage profiles for stainless steel projectile shots . . .	14
Figure 5. Shot 53 back plate	17
Figure 6. Shot 67 back plate	19
Figure 7. Shot 85 back plate	21
Figure 8. Disrupter damage comparison of shots 53 and 67	25
Figure 9. Disrupter damage comparison of shots having the baseline layered shield configuration	25
Figure 10. Debris distance through disrupter versus time	26
Figure 11. Disrupter damage comparison of shots 84 and 85	27
Figure 12. Flash x-ray of shot 53 at 28 μ sec	28
Figure 13. Flash x-ray of shot 55 at 28 μ sec	28
Figure 14. Flash x-ray of shot 77 at 31 μ sec	29
Figure 15. Flash x-ray of shot 85 at 31 μ sec	29
Figure 16. Front hole size versus plate thickness	31
Figure 17. Disrupter damage comparison of shots 65 and 66	34
Figure 18. Disrupter damage comparison of shot 83 with 55 and 77	35
Figure 19. Problem 8.22 shield geometry with model boundaries	45
Figure 20. Problem 8.44 shield geometry with model boundaries	46
Figure 21. Problem 8.64 shield geometry with model boundaries	46
Figure 22. Density plots of total shield model (8.22 and 8.44) at 0.8 μ sec.	48

Figure 23. Projectile density profiles to show shock wave progression during front plate penetration	49
Figure 24. Projectile density profiles to compare normal and yawed impact at 2 μ sec.	51
Figure 25. Projectile profiles to compare double cone (2D) to the yawed cylinder (3D) at 2 μ sec.	53
Figure 26. Projectile density profile at 10 μ sec; comparison of double cone and normal incidence cylinder	55
Figure 27. Projectile density profiles at 2 μ sec; comparison of double cone debris cloud versus front plate thickness	57
Figure 28. Projectile density profiles at 10 μ sec; comparison of double cone debris cloud versus front plate thickness	59
Figure 29. Comparison of sphere and normally incident cylinder debris clouds at 2 μ sec	61
Figure 30. Comparison of sphere and normally incident cylinder debris clouds at 10 μ sec	63
Figure 31. Front plate debris for problems 8.74 and 8.64 at 10 μ sec.	66

ABSTRACT

During the 3-year period of 1987 through 1989, the Advanced Shield Phenomenology Program included a research and development effort, with both experimental work and analytical support, to design a low weight, survivable shield against a stainless steel projectile at low earth orbit velocity. The specific threat used was a 1.75 gram, length to diameter ratio of one, stainless steel cylinder. The impact velocity was ~ 7 km/s.

Testing was performed at the Arnold Engineering Development Center, Arnold Air Force Base, Tullahoma, Tennessee. Sixteen shield configurations were tested. The Hull hydrocode was used for detailed analysis of five impact configurations. A successful shield was designed, which had a stainless steel front and back plate and 15.24 cm of carbon felt disrupter. The success of this configuration against the stainless steel threat was repeated. In comparison with the solid homogeneous aluminum shield necessary to stop the same threat, the layered shield developed has an areal density (mass per unit area) of 15.7% of the solid aluminum shield. Six conclusions of particular interest from the stainless steel work are summarized briefly as follows:

1. The yaw angle of a cylindrical projectile at impact has a significant effect on shield survivability.
2. Areal density alone may not be enough to adequately model front plate behavior; thickness and material should be considered as separate variables.
3. Stainless steel very possibly is more damaging than can be accounted for by its density alone.
4. A double-layer front plate produced no significant change in survivability.
5. Analytical results and test results are overall in excellent agreement.
6. Hydrocode analysis is a useful tool in design and development of hypervelocity shields.

1. INTRODUCTION

This report covers the research and development efforts performed to design a layered composite shield to protect against a stainless steel threat at low earth orbit speeds. Included here are the experimental work and the supporting analyses, which combined to produce a survivable shield of low areal density. The particular threat used in this study was a stainless steel cylinder, with a mass of 1.75 grams and a length to diameter ratio of one. The impact velocity was 7 km/s. Sixteen tests

and five analyses configurations were completed during the study. Testing consisted of firing a cylinder, as described above, into a layered shield configuration. For each test, the incident velocity was held constant at 7 km/s, and the projectile line of flight was kept perpendicular to the front shield surface. Front plate thickness and other design parameters were changed, both to optimize shield design for low weight and improved performance and to study the phenomenology of stainless steel hypervelocity impact. Experimental procedures, test hardware, and test results are described and discussed fully in the report sections so entitled. The hydrocode analysis covered in this report was initiated after nine tests to further study an apparent inconsistency in the test results. Two identical shield configurations had, when tested, produced widely different back plate damage. The yaw angle of the projectile was thought to possibly be the cause of the lack of repeatability. The Hull hydrocode analysis was used to compare the projectile breakup for the zero yaw orientation, where the flat plate and flat cylinder face are in full contact, to the case of projectile impact with the projectile centerline rotated to a yaw angle of 45 degrees. To complete the analytical study, a third case analysis was made for a spherical projectile of identical mass and impact velocity. Analytical methods and results are presented and discussed in the appropriate report sections following.

Also included in this report are comparisons of analytical and experimental results, conclusions reached as a result of this study, and recommendations for further work in this area.

2. EXPERIMENTAL PROCEDURE

Testing was conducted at the Arnold Engineering Development Center at the Arnold Air Force Base in Tullahoma, Tennessee, using the S-1 Range Light Gas Gun. Data were taken in several areas, working in coordination with the S-1 Range personnel, including hard and soft flash x-rays and strain gage readings. The detailed test and data acquisition methods are covered fully in a separate report devoted to the subject (Smith, in press) and are thus not included here.

A discussion of the experimental design logic used during testing is included in this report. This experimental design procedure was initiated as part of the Fast Track Shield Program (ORNL Staff, 1989) and was further developed during this study. The basic element of this experimental procedure is flexibility during testing. To achieve this flexibility, which in turn allows rapid development of a shield design, a test matrix is developed before testing, rather than a list of specific configurations to be tested. An example of a matrix used during a test series is shown in Figure 1. Design decisions can be made at any time during a test series, allowing use of all known experimental results, especially those of the immediately previous test(s).

Decisions made during testing were based on experimental results that indicated certain performance levels. The term "gross failure," seen in Figure 1 as a directional indicator on the test matrix, was used to describe a shield back plate with a large hole having large petals. A gross failure mandated a change in shield stackup such as a different front plate or more disrupter. The criterion for success was that of a back plate which had bulged or deformed but had not been perforated in any way. A back shield that had bulged, but had pinhole perforations, was nearly successful, indicating only minor changes in shield configuration. As the testing continued, consideration of changes to be made also incorporated the evaluation of yaw angle at impact. This

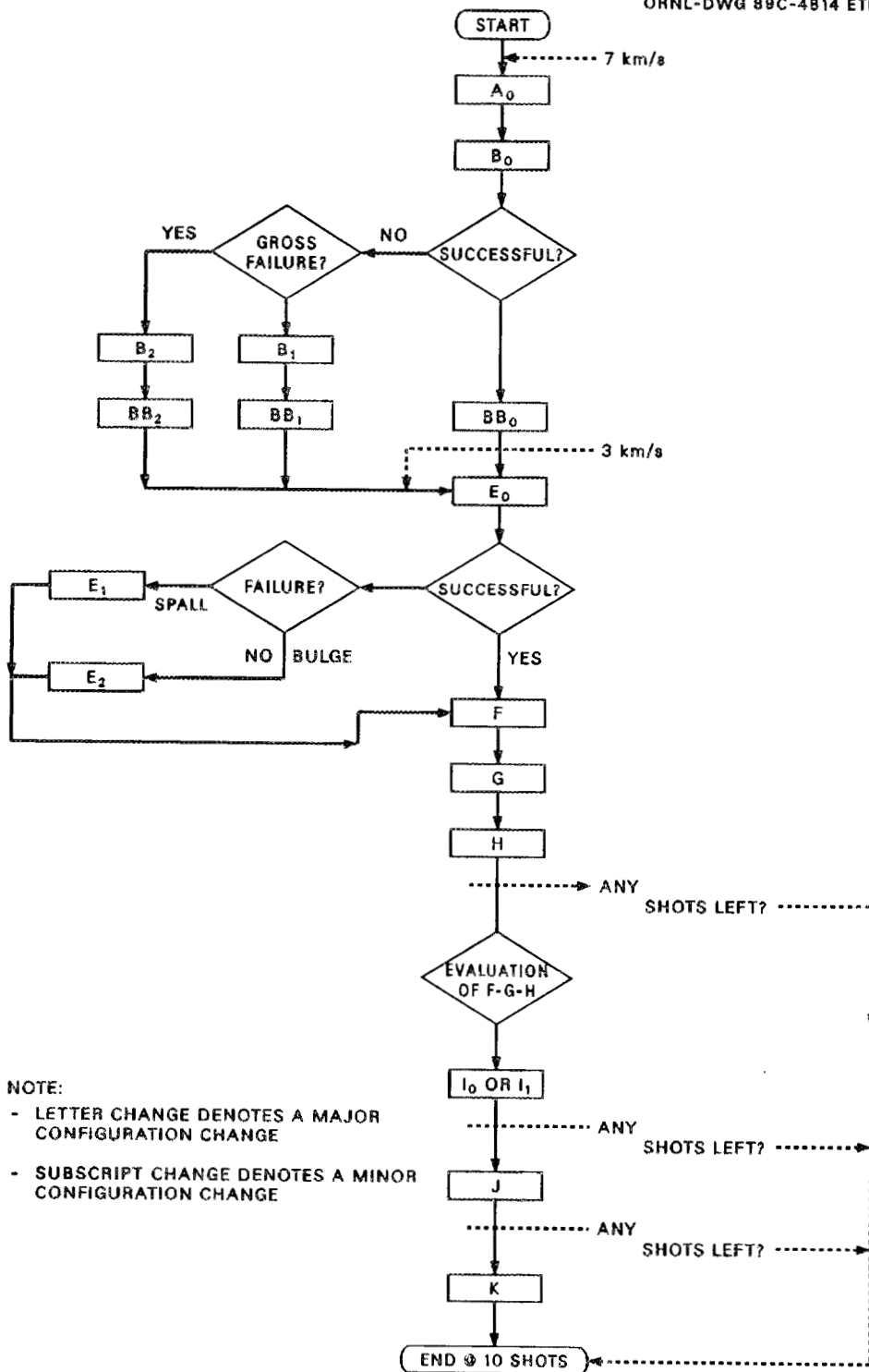


Figure 1. Experimental test decision matrix

was a further development of the design procedure and is discussed more fully in later report sections.

The stainless steel study was a major portion of the total Advanced Shield Phenomenology Program effort. The experimental work took place over a period of three years and included shots during four test series. Test series 4, in 1987, included three stainless steel projectile shots. Test series 5 was conducted in early 1988 and also included three stainless steel tests. Series 6, later in 1988, included four stainless steel tests. The final series, number 7, performed in early 1989, was composed of over 50% stainless steel tests, using six of eleven shots on this problem. Between test series, detailed evaluation and analysis of test results were continued. The difficulty of countering the stainless steel threat can be seen from the time and effort necessary to obtain a successful, low weight, shield design. Analysis efforts were used extensively in support of the experimental work and were especially useful in evaluation of the effect of projectile yaw angle at impact for the cylindrical projectiles used.

3. TEST HARDWARE DESCRIPTION

A total of 16 tests were performed using a 1.75 gram stainless steel projectile at an impact velocity of 7 km/s (nominal). The following paragraphs briefly describe the shield configurations used in each test. Hardware summaries are given in Table 1, including specific thicknesses, materials, and weights. Comparison of shield hardware is given in Table 2 for ease in identifying test setups with repeated parameters, such as similar front plates.

Shot 49. A solid aluminum (6061T0) shield, 8.382 cm thick with an areal density of 22.79 gm/cm², was used to provide the reference thickness for further weight reduction.

Shot 50. The baseline layered shield configuration was used in this shot, consisting of a 304L stainless steel front plate, porous carbon felt disrupter, and a 304L stainless steel back plate. A 12.7 cm (5-inch) spacing between front and back plates was used. Also, a thin layer of polyurethane was included on the rear surface of the back shield.

Shot 53. Again, a 304L stainless steel front plate and porous carbon felt disrupter were used. A 21-6-9 stainless steel back plate was part of the shield stackup for this test and all subsequent stainless steel projectile tests up to shot 84. The layer of polyurethane "spall catcher" was omitted on this and all succeeding metal projectile tests. On this and all later stainless steel projectile shots, the spacing between front and back plates was increased to 15.24 cm (6-inch).

Shot 55. The basic layered configuration was used here, very similar to shot 53, with minor variations in layer thicknesses.

Table 1. Hardware summary for stainless steel projectile shots

Shot No.	Front Plate		Disrupter			Back Plate		Total A.D. [*] g/cm ²	% Reference shield
	material	t ^{**} , cm	material	spacing, cm	A.D. [*] , g/cm ²	material	t, cm		
49	6061T0	8.382	-	-	-	-	-	22.79	100.00
50	304L	0.097	felt	12.70	1.09	304L	0.097	2.762	12.12
53	304L	0.102	felt	15.24	1.20	21-6-9	0.069	2.527	11.09
55	304L	0.114	felt	"	1.07	"	"	2.542	11.15
58	304L	0.097	wool	"	0.99	"	"	2.324	10.20
60	304L	0.099	wool	"	1.31	"	"	2.660	11.67
64	21-6-9	0.069	felt	"	1.20	"	"	2.224	9.76
65	304L	0.076	felt	"	1.52	"	"	2.641	11.59
66	2024T3	0.224	felt	"	1.22	"	"	2.652	11.64
67	304L	0.094	felt	"	1.04	"	"	2.482	10.89
74	304L	0.122	wool/felt	"	1.04	"	"	2.564	11.25
75	304L	0.119	B-cloth	"	1.10	"	"	2.559	11.23
77	304L	0.152	felt	"	1.05	"	"	2.781	12.20
83	21-6-9	2X0.070	felt	"	1.20	21-6-9	0.069	2.825	12.40
84	304L	0.173	felt	"	1.20	304L	0.122	3.559	15.62
85	304L	0.173	felt	15.24	1.21	304L	0.122	3.568	15.66

NOTE: All witness plates were 0.3 cm aluminum, located 2.54 cm behind the back shield

^{*}A.D.: areal density; the mass per unit area

^{**}t: thickness

Table 2. Comparison of shield hardware

Front Plates		Disruptor				Back Plates		Total Shield A.C.	
t ^{**} , cm	shot no.	material	shot no.	A.D., [*] g/cm ²	Shot no.	t ^{**} , cm	shot no.	A.D., [*] g/cm ²	shot no.
0.069	64	felt	50,53,55, 64,65,66, 67,77,83, 84,85	1.0± .004	58,74	0.069	53,55,58, 60,64,65, 66,67,74, 75,77,83	2.224	64
0.076	65	wool	58,60	1.07± .003	50,55,64,75,77	0.097	50	2.324	58
0.099± .005	50,53,58, 60,67	felt/wool	74	1.20± .002	53,67,83,84,85	0.122	84,85	2.52± .04	67,53,55, 74,75
0.119± .005	55,74,75	B-cloth	75	1.31	60			2.65± .01	60,65,66
0.140	83			1.52± .002	65,66			2.77± .01	50,77,83
0.152	77							3.56± .01	84,85
0.173	84,85								
0.224 (A)	66								

*A.D.: Areal density; the mass per unit area

**t: thickness

Shot 58. The test configuration for shot 58 included stainless steel front and back plates as in earlier tests. However, a steel wool disrupter was inserted rather than the carbon felt as before.

Shot 60. This shot was very similar to shot 58, with the only difference being a greater amount of steel wool disrupter included in the same 15.24 cm space.

Shot 64. Again, the basic configuration of stainless steel front and back plates with porous carbon felt disrupter was used. A 21-6-9 rather than a 304L stainless plate was the front shield layer for this test. As given in Table 1, this was the thinnest of the front shields used.

Shot 65. The configuration for shot 65 also used the basic shield of stainless steel- carbon felt- stainless steel, with minor variations in layer thicknesses and disrupter density.

Shot 66. The main point of interest concerning the shield stackup for shot 66 is that it is identical to that of shot 65, except that the stainless steel front layer of shot 65 was replaced with an identical areal density (but much thicker) front shield of 2024T3 aluminum.

Shot 67. Shot 67 was a repeat of shot 53.

Shot 74. For shield 74, stainless steel front and back plates were again used. The disrupter differed from any previous ones in that the first half was steel wool with the back half of carbon felt. The measurement of "half" was based on areal density rather than thickness.

Shot 75. This shot also used similar front and back plates with a very different disrupter material. Ceramic fabric layers were evenly spaced across the 15.24 cm to provide the disrupter.

Shot 77. The basic shield setup was used with small variations in layer thicknesses and disrupter densities.

Shot 83. The main difference from the basic setup for this shot was that the front layer was actually a double layer of two thin 21-6-9 stainless steel layers. The two layers were held together by the test holder hardware but were not glued. A carbon felt disrupter and stainless steel back plate were used.

Shot 84. The basic shield setup of stainless steel - carbon felt - stainless steel was again used. However, the back shield thickness was increased from the thicknesses used in any previous tests, and the material was 304L rather than 21-6-9 stainless steel. The front shield was also thicker than any previously tested. Again, detailed configurations are given in Table 1.

Shot 85. This shot was a repeat of shot 84.

4. TEST RESULTS DESCRIPTION

Results for all sixteen tests are presented and briefly described in this section. Also included is yaw angle of the projectile at impact, although this parameter is actually a test variable which cannot be controlled rather than an actual result.

Yaw Angle at Impact. This variable, as previously mentioned, is not controllable during projectile launch. The exact orientation of the cylindrical projectile as it strikes the target shield, while occurring during the test and thus being one of the test variables, is only known after the test from flash x-ray analysis and from the front plate damage configuration. A certain amount of uncertainty remains after the x-ray analysis due to the small distance left for the projectile to travel after the last orientation information is obtained. The projectile yaw rate over this distance is unknown, thus creating the uncertainty mentioned. Figure 2 shows the convention used in specifying yaw angle. Table 3 includes the yaw angle of the cylinder at impact for each test and

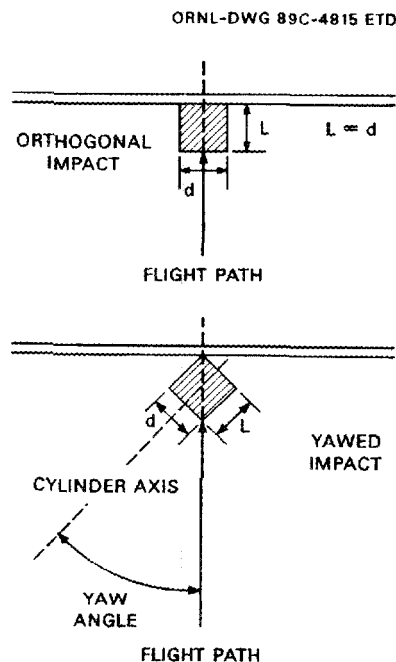


Figure 2. Yaw angle nomenclature

Table 3. Yaw angle at impact for stainless steel projectile tests

Shot Number	Yaw angle, degrees	Uncertainty, degrees
49	55	+4
50	59	+4
53	8	+8
55	60	+4
58	69	+4
60	52	+4
64	13	+4
65	42	+4
66	41	+4
67	17	+8
74	42	+8
75	42	+2
77	78	+4
83	45	+4
84	14	+2
85	78	+4

an estimate for each of the uncertainties involved. At this point, yaw angle is simply presented as one of the variables involved; later discussion evaluates its importance.

Front Plate Results. For each test, the front plate hole was carefully measured. Results measured included maximum, minimum, and average hole diameters. The hole area was calculated using average diameter. These results are given in Table 4. Front plate holes varied in size and shape. Each hole is shown in Figure 3, which also includes for quick reference the plate thickness and average hole diameter.

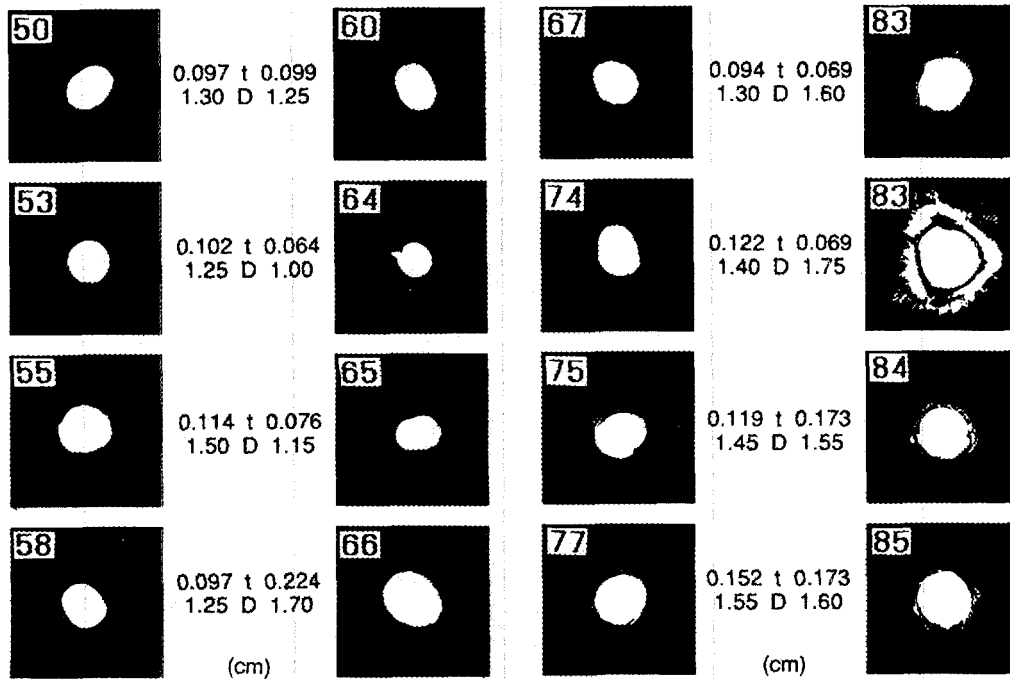
Disrupter Damage Profiles. For the fifteen shots which incorporated a disrupter material, damage profiles in the disrupter are shown in Figure 4. Measurements were made for each material layer of the minimum, maximum, and average hole radius as well as the maximum spread of blast

Table 4. Front plate results

Shot Number	t^a cm	D_{avg}^b cm	D_{max}^c cm	D_{min}^d cm	Area cm ²	D_{avg}^b/d^e	t^a/d^e
50	0.097	1.30	1.50	1.15	1.327	1.98	0.15
53	0.102	1.25	1.30	1.25	1.227	1.91	0.16
55	0.114	1.50	1.60	1.40	1.767	2.29	0.17
58	0.097	1.25	1.40	1.15	1.227	1.91	0.15
60	0.099	1.25	1.50	1.10	1.227	1.91	0.15
64	0.064	1.00	1.00	1.00	0.785	1.52	0.10
65	0.076	1.15	1.40	1.00	1.039	1.75	0.12
66	0.224	1.70	1.90	1.50	2.270	2.59	0.34
67	0.094	1.30	1.45	1.25	1.327	1.98	0.14
74	0.122	1.40	1.50	1.20	1.539	2.13	0.19
75	0.119	1.45	1.60	1.30	1.651	2.21	0.18
77	0.152	1.55	1.65	1.50	1.887	2.36	0.23
83	0.139	1.60	1.80	1.40	2.011	2.44	0.21
84	0.173	1.55	1.60	1.50	1.887	2.36	0.26
85	0.173	1.60	1.75	1.55	2.011	2.44	0.26

- ^a thickness
- ^b average hole diameter
- ^c maximum hole diameter
- ^d minimum projectile diameter
- ^e projectile diameter

ORNL-DWG 89-4816 ETD



t = PLATE THICKNESS
 D = AVERAGE DIAMETER

Figure 3. Front hole results

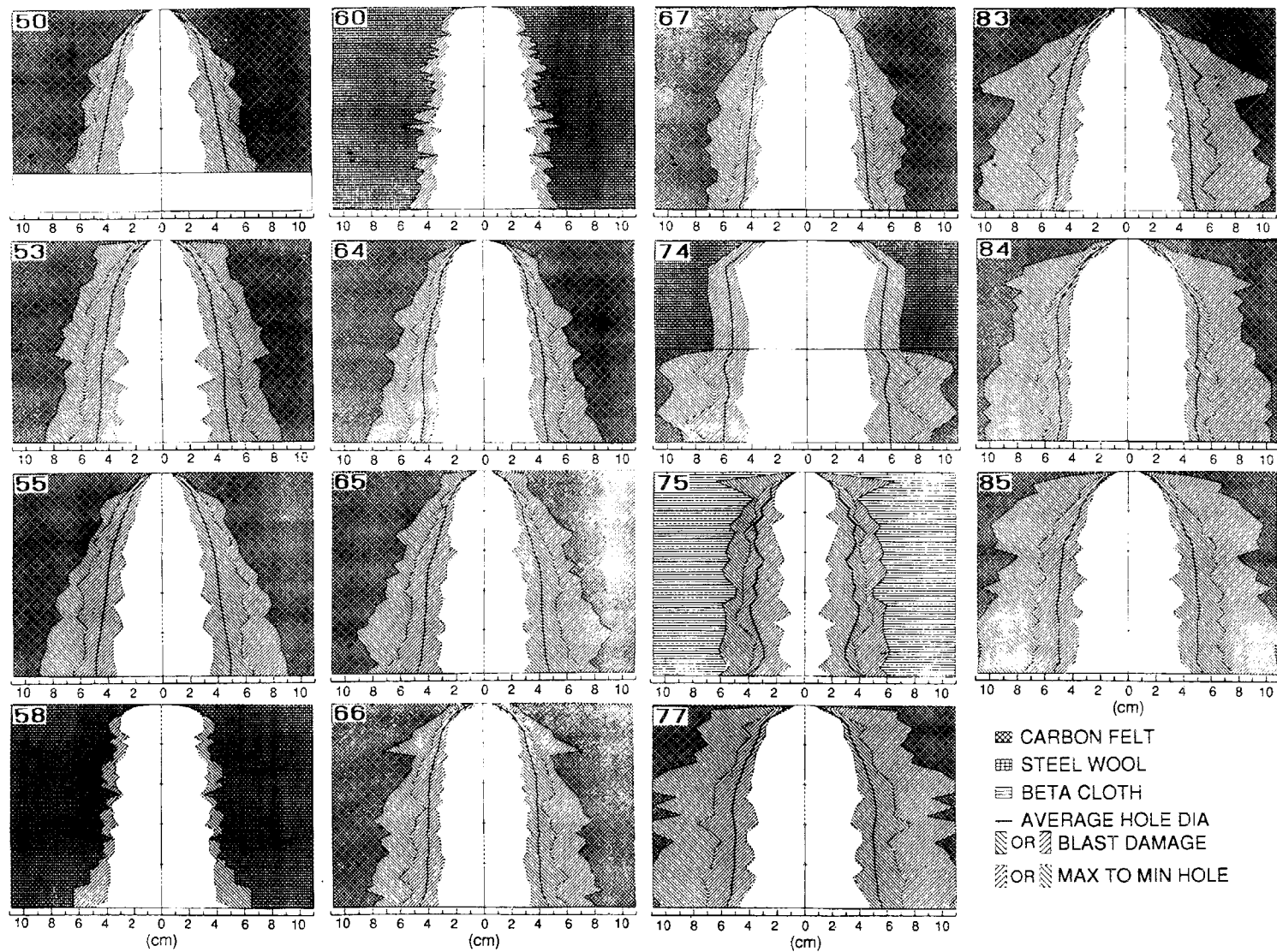


Figure 4. Disrupter damage profiles for stainless steel projectile shots

damage. Discussion and comparisons of the disrupter damage profiles are included in one of the following report sections.

Back Plate Results. Table 5 contains a summary of back plate results. The damage to the back plate of each test shield stackup is more fully described below in order of shot number.

Table 5. Summary of back plate results

Shot Number	Back Plate Damage Description	Time from impact to back plate, μ sec
49	Bulge, 0.95 cm high; F. Crater, 4.45 cm Dia., 3.77 cm deep	N.A.
50	Large hole, 8.89 x 7.62 cm, 5 petals	22-32
53	Bulge + 3 small petaled holes	56
55	Large hole, 10.2 x 5.1 cm, 5 petals	39
58	Large hole, 12.5 x 9.4 cm, 5 petals	35
60	X-large hole hole, 14 x 9.5 cm, 6 petals	39
64	Large hole, 14.5 & 11 cm (cross corners), 4 petals	40.3
65	Large hole, -10 x 7 cm, 4 petals	30 +/-1
66	Large hole, 10.5 x 6 cm (cross corners), 6 petals	36 +/-1
67	Large hole, 8 x 4.5 cm, 6 petals (irreg.)	40 +/-1
74	Large hole 9 x 12 cm, 5 petals, (irreg.)	33 +/-2
75	Large hole, 8 x 12 cm, 5 petals (irreg.)	36 +/-2
77	Gash, 6 cm long, 1 cm wide (big end) + 5 small pinholes	43
83	Large hole, 8 cm (cross corners), 4 petals	41
84	Success! SS proj., 2 cm high bulge + 5 small bulges	51 +/-4
85	Repeat shot 84, Good! 2 cm H bulge + 9 very small bulges	58

Shot 49. The front crater created in the solid aluminum measured 3.8 cm deep and 4.5 cm in diameter. On the back surface of the shield, a bulge 0.95 cm high resulted.

Shot 50. A major failure of the back plate occurred. The center of the plate appeared to have been hit with a closely packed group of small pellets, similar to the appearance of a close-range shotgun blast. A large hole, approximately 9 x 7.5 cm, resulted, having 5 large petals. The tips of the petals show the blast impact; the sides of the petals are clean tears.

Shot 53. The back plate of this shot indicated a near success. An overall bulge was produced with one very small and two small petalled holes visible from the rear. This plate is shown in Figure 5. Another indication of near success is the fact that the mounting holes used around the edge of the plate show the beginnings of yield against the mounting screws used. This result is only seen in those plates which have been subjected to a blast pressure pulse which results in the characteristic bulge of a successful shield. A witness plate of thin aluminum was included 2.54 cm behind the back plate for this and subsequent tests. For shot 53, the witness plate had very minimal damage.

Shot 55. The back plate for shot 55 failed with the resulting damage being very similar to shot 50. The five petals which were produced show a "connect-the-dot" appearance on the tips, so that if the petals were pushed back into a flat plate, the damage on the edges would match back into the holes produced by the debris impact. There are several small craters on the inner surface of the petals; one petal has a small hole which is also petalled. Clearly, the back plate withstood impact of a portion of the debris cloud, until

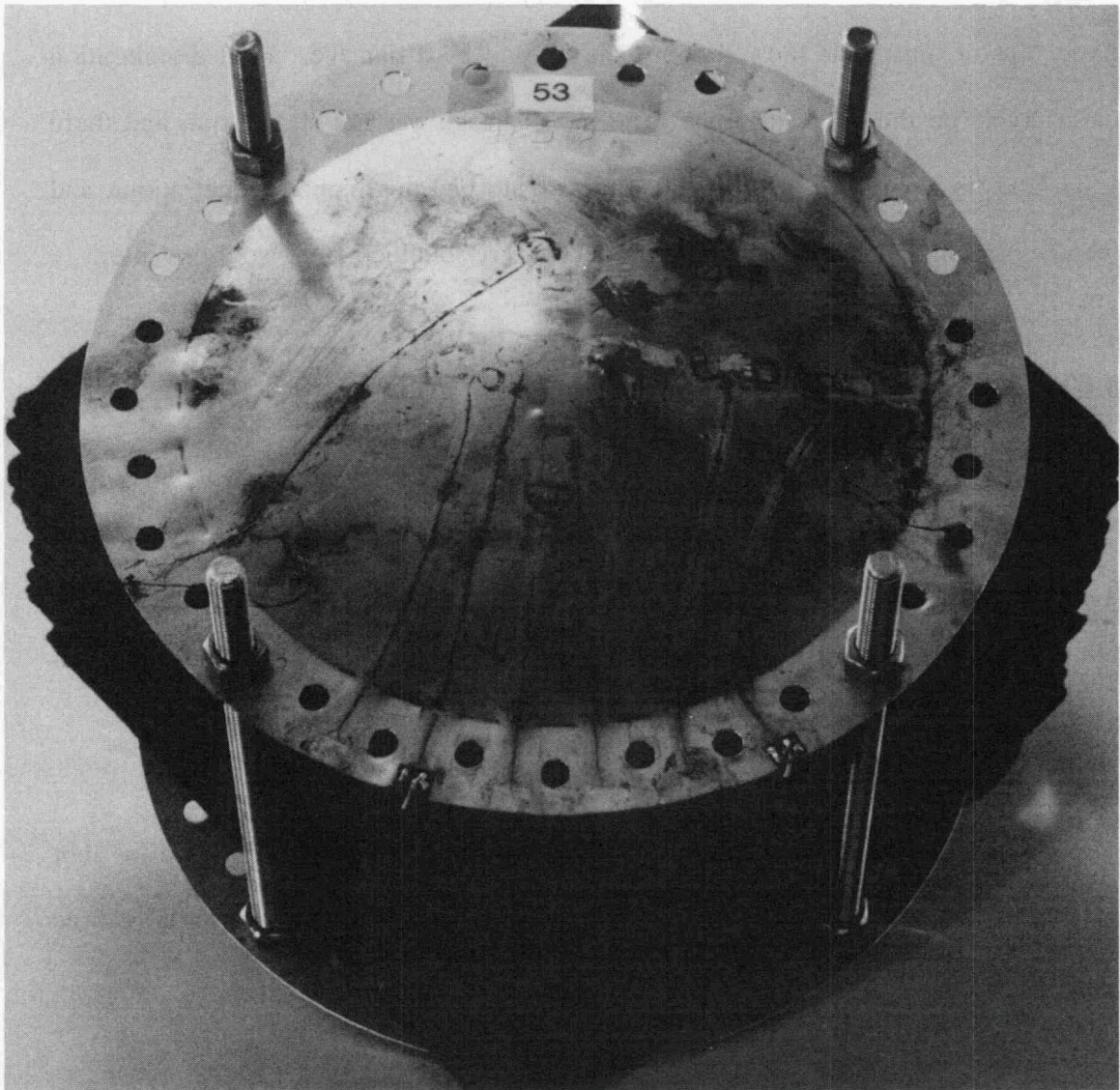


Figure 5. Shot 53 back plate

too many small perforations caused failure under the remaining blast. The blast damage for shot 55 was more spread out than for shot 50. Witness plate damage was slight, but more than for shot 53, having a bulge and a few small craters as well as a liberal coating of carbon dust.

Shot 58. Again, the back plate failed and a large hole with large petals was produced. The very tips of the petals showed debris impact and blast damage. Heat discoloration was also visible on the petal tips only. The blast damage was not spread out, and there were no holes in any of the petals. The witness plate had two pinhole penetrations, and the center portion was coated with melted and then re-solidified steel wool disrupter.

Shot 60. The results of this shot were very similar to the results of shot 58. A slightly larger back plate hole was produced.

Shot 64. Results for shot 64 look very similar to those of shot 55. Looking at the back side of the shield, one petal has two small bulges, one of which has split but not petalled. The witness plate also is very similar to that of shot 55.

Shot 65. Again, the results for this back plate are very similar to the back plate for shot 55. However, the witness plate for shot 65 was seriously perforated, having a large hole and a small one.

Shot 66. Although the hole produced was measurably smaller, the results for this shot's back plate and witness plate are otherwise very similar to those of shot 65.

Shot 67. This shot setup was a repeat of shot 53. Results, however, match those of shots 55, 64, 65, etc., rather than those of shot 53. The back plate for shot 67 is shown in Figure 6.

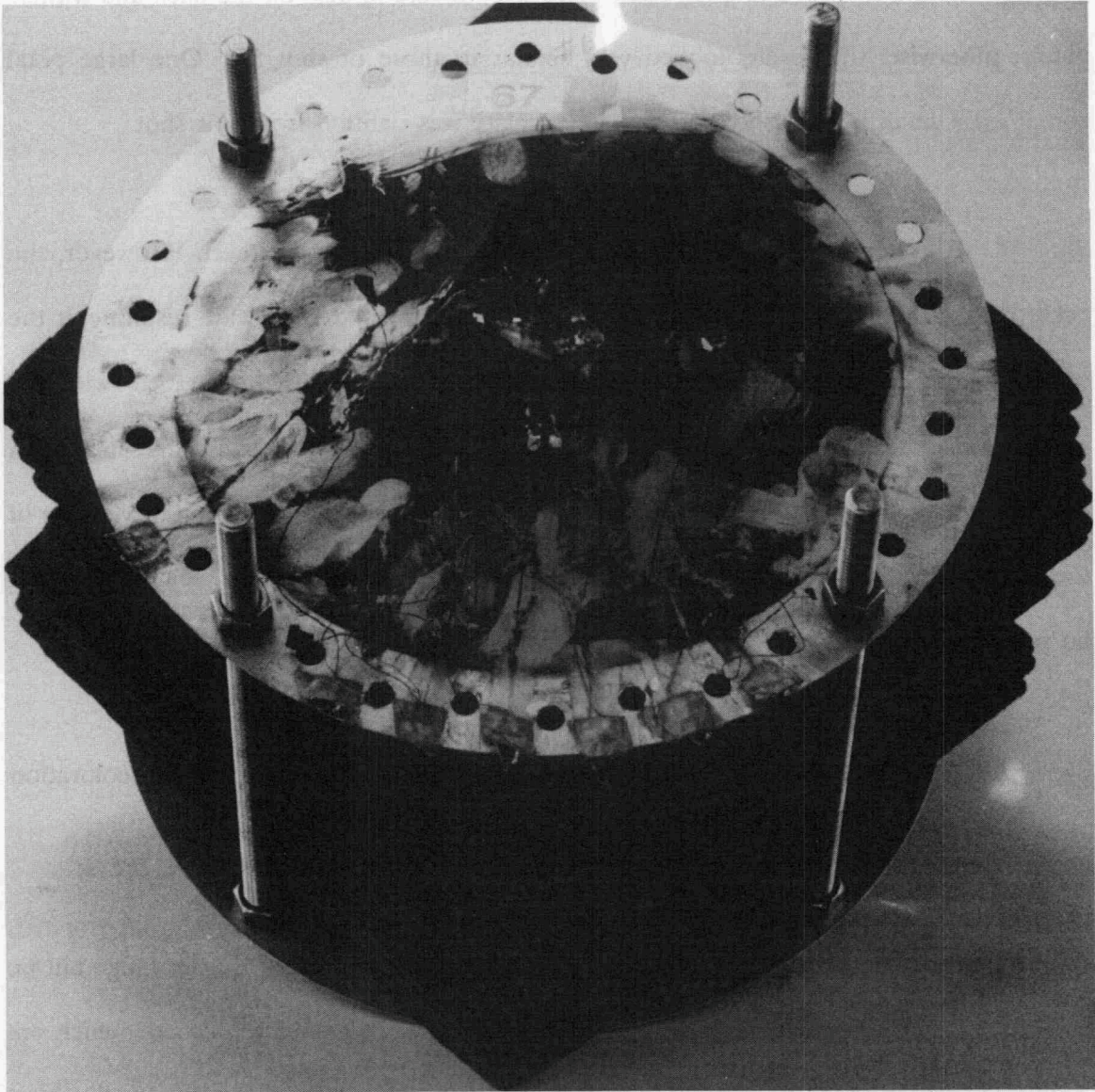


Figure 6. Shot 67 back plate

Shot 74. The back plate of this shot looks very similar to the plates of shots 55, 64, 65, etc. but differs from the results of shots 58 and 60 in that there is no evidence of the steel wool portion of the disrupter on the witness plate. A penetration of the witness plate did occur.

Shot 75. With a B-cloth disrupter used, there was no carbon dust on the back and witness plates; otherwise, the results looked very similar to those of shot 55. One large petal contained a small petalled hole. The witness plate was omitted from this shot.

Shot 77. An overall bulge of the back shield was produced by this test. However, the back plate also split, with a long triangular gash 6 cm long and 1 cm wide resulting at the center of the bulge. This gash has a definite "connect-the-dot" appearance, with the matching small hole sections concentrated at the wide end of the split. Further indication that the shield configuration tested was close to a success was the beginning of yielding of the mounting holes. The witness plate was bulged and had a few very small craters but no penetrations.

Shot 83. This shot had similar results to those of shot 50, except for heat discoloration of the witness plate. The witness plate was penetrated.

Shot 84. The back plate met the qualification of success, having a significant bulge but no penetration. There are several very small bulges on the large bulge, two of which are noticeably larger than the others. On the inside surface of the back shield, the blast damage is quite spread out, showing up as very small craters full of carbon dust.

Shot 85. This shot was a repeat of shot 84 with almost identical results. The back plate has the same overall bulge with very small bulges scattered across the surface. Shot 85 has more of the small bulges, all of which are very small. Again, the blast damage was quite spread out over the shield surface. For shots 84 and 85, the mount holes showed no sign of incipient yield. Figure 7 is a picture of the rear surface of shot 85.

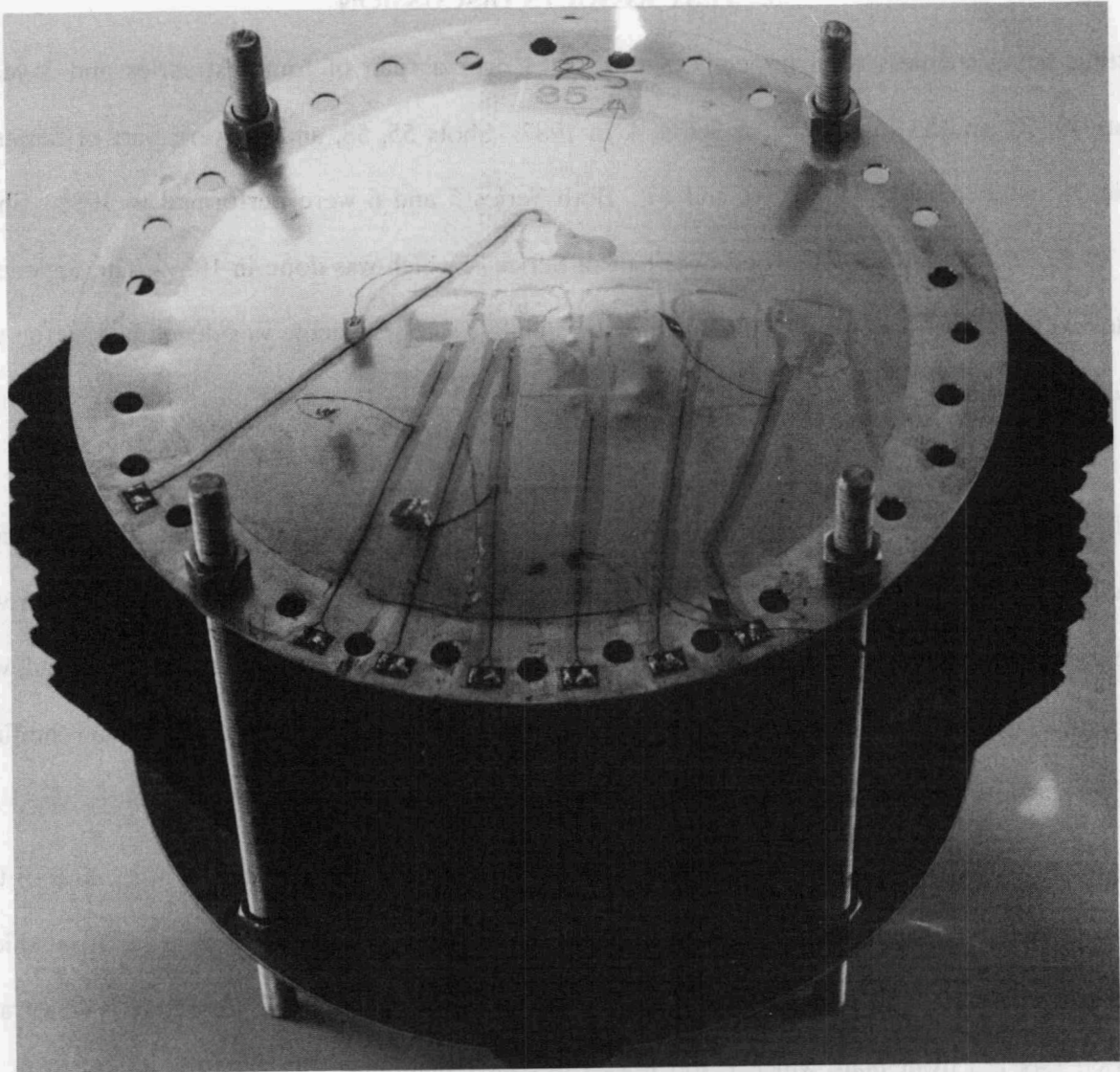


Figure 7. Shot 85 back plate

5. TEST RESULTS DISCUSSION

Testing, using stainless steel projectiles, took place over a span of four test series and 3 years. Shots 49, 50, and 53 were done in Series 4, in 1987. Shots 55, 58, and 60 were part of Series 5. Series 6 included shots 64, 65, 66, and 67. Both Series 5 and 6 were performed in 1988. Shots 74, 75, 77, 83, 84, and 85 comprised over half of Series 7, which was done in 1989. The logic used in development of a successful shield against the stainless steel projectile was developed as the test series continued.

At the initiation of testing against a stainless steel threat, shield design logic similar to the design logic used in earlier successful layered shields against lexan, aluminum, and tantalum-tungsten was employed. Shot 49, providing the baseline reference for a solid homogeneous aluminum shield, was not significantly different from design expectations. Only one shot was necessary to obtain the final shield thickness for bulge without spall. Configurations for shot 50 and 53 were also based on previously used logic. Basically, the front shield was specified in the region of 15% to 20% of the projectile diameter, to provide the necessary breakup of the projectile, and to keep the front shield as thin as possible. This both minimizes weight and, as discussed by earlier researchers (Hart and Wessel, 1986), a front plate which is too thick can cause high-density pieces of front shield to be part of the debris cloud and thus cause back plate failure. Due to the near-success of shot 53, the next series tested shields very similar in configuration. Shot 55 had a slightly thicker front shield, and Shots 58 and 60 used the same thickness and material front shield but a different disrupter. Steel wool had performed very satisfactorily as a disrupter against the tantalum-tungsten threat. The gross failure of these three shields led to the conclusion that the design had moved away rather than toward the optimum. Again, this used shot 53's near-success as being very close to the optimum. Based on this logic, the next test series used front plates of less areal density than shot 53. Shots 64 and 65 were thinner plates of stainless steel while shot 66 was aluminum and,

therefore, was much thicker even though the areal density equalled shot 65. At this point, the failure of these three shields indicated a problem of some sort. The evident closeness of shot 53 to the optimum design had been used as a basis up to this point but, with the failure of designs on both sides of 53 on the response surface, further evaluation was necessary.

Shot 67 was set up to be a repeat of shot 53. As previously seen in the results description, the near success of shot 53 did not repeat. Shot 67 was a gross failure. In all previous testing, shot repeatability had been periodically checked and had not been a problem. Serious thought and considerable analysis went into the resolution of this problem. The analytical work done is presented and discussed in Sections 6-9. The analytical work caused a re-evaluation of the experimental results. The conclusion was made, based on both analytical and experimental results, that the yaw angle of the stainless steel cylinder at impact should be considered as a factor in shield performance. Further discussion in the following paragraphs both explains and uses this theory in coverage of the experimental results.

The basic function of the front plate is to break up the projectile as completely as possible. The state of the resulting debris cloud is extremely important. Optimally, the debris cloud should be composed of low-density, very small particles. This corresponds to vaporization of the projectile with the disrupter then slowing the cloud down enough for the back plate to withstand the blast impulse. Ideally, the breakup of the projectile also spreads the debris cloud out over a wide area. Thus the load is distributed over the back plate, and the chance of back plate survival increased. Two primary front plate factors, (given a specified projectile and velocity) at the onset of testing, were thought to determine the debris cloud state, velocity reduction, and spread. First, the thickness of the plate affects both the breakup of the projectile and the spread of the resulting

debris. The material used for the front shield also affects the debris generated. Together, the material density and thickness are combined as the areal density, but test results are more consistently explained by considering two separate variables rather than lumping them together as areal density. This will be discussed further later in the report. After Series 6, the effect of yaw angle was added as a factor. Using these three factors, the near-success and apparent non-repeatability of shot 53 are now consistently explainable.

As seen in Figure 3, front plate holes vary in size and shape. The elliptically shaped holes correspond to impacts at yaw angles which deviate from an exactly orthogonal impact (0 degree yaw), as shown in Figure 2. Shot 53 has very nearly a 0 degree impact, while the impact for shot 67 occurred at approximately 20 degrees. As discussed in the analytical results, the type impact of shot 53 results in a lower density debris cloud. The impact of shot 67 is closer to that of the "worst case" impact of a 45 degree yawed projectile. Front plate thickness and material effects were consistent between the shots. This consistency is shown in Figure 8, a comparison of the disrupter damage profiles of shots 53 and 67. The two profiles are very similar in spread, an expected result due to the same thickness and material of the front plate. Figure 9 compares the disrupter damage for all shots having the basic shield setup of stainless-felt-stainless stackups. Again, the spread of the debris clouds is consistent with plate thickness and material. The difference between 53 and 67 is resolved by the difference between their front hole shapes, indicating the difference in debris cloud state.

A further effect of the 0 degree yaw angle is indicated in Figure 10, a plot of time versus travel through the disrupter material. Shot 53 fits with the success/near-success group, rather than with the group having similar front plates. The indication is that the velocity reduction across the front plate was greater. This is caused by a thicker plate or by a very low yaw angle.

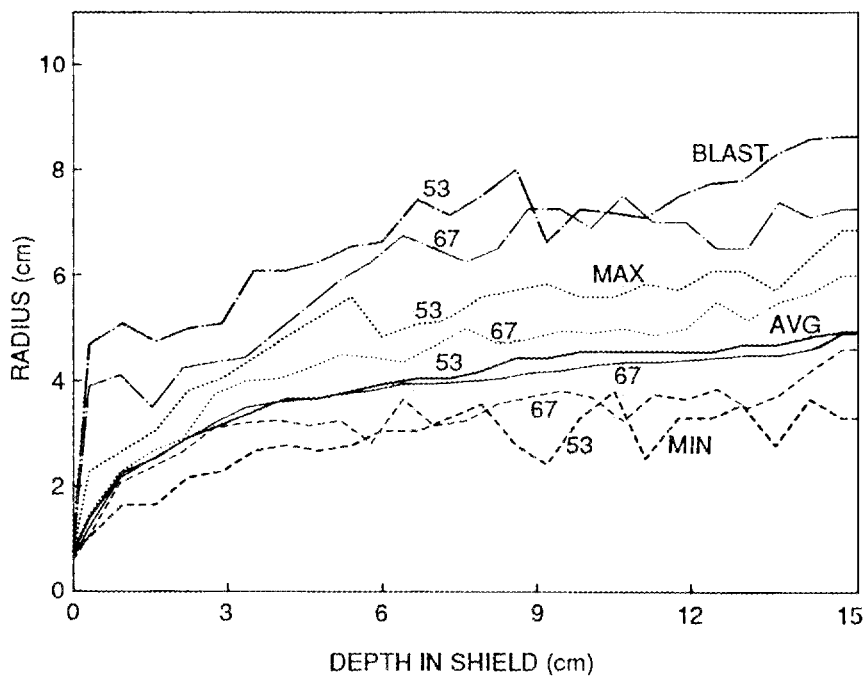


Figure 8. Disrupter damage comparison of shots 53 and 67

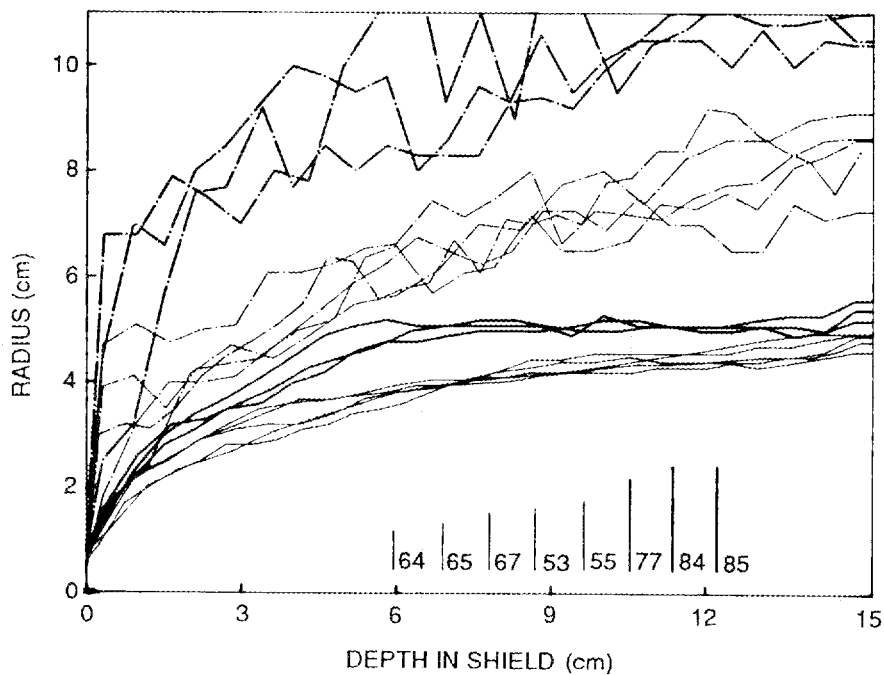


Figure 9. Disrupter damage comparison of shots having the baseline layered shield configuration

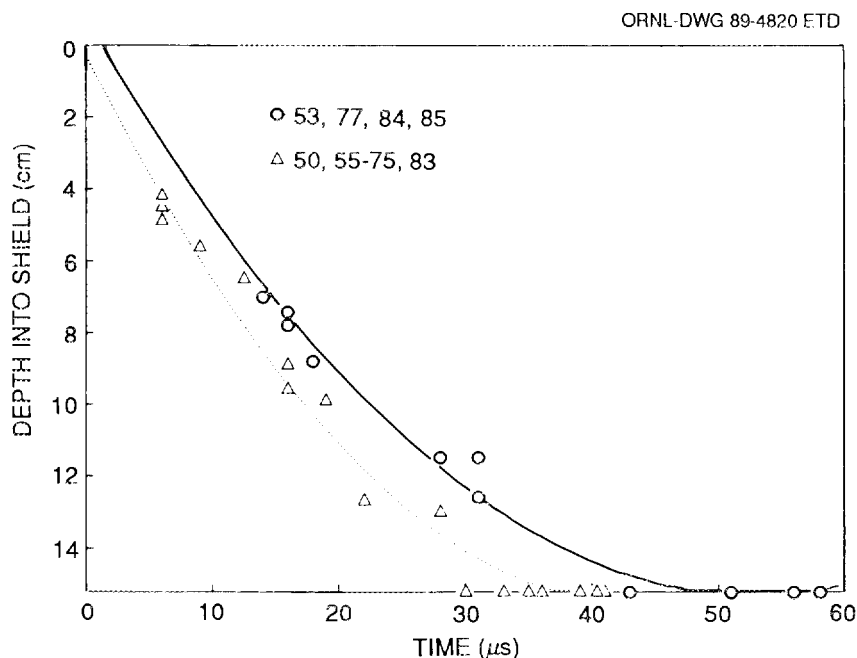


Figure 10. Debris distance through disrupter versus time

Another, more minor, test discrepancy can be resolved by consideration of the yaw angle at impact. This is the survival of shot 64's witness plate, even though the front shield was the thinnest tested and witness plates for other shots using much thicker front plates were penetrated. From evaluation of the front holes shown in Figure 3, the hole in front shield 64 is an almost perfect circle, indicating a yaw angle close to 0 degrees.

Using the idea that a 0 degree yaw would at least partly negate the effects of a too-thin front plate, Series 7 shield configurations incorporated thicker front shields to compensate for more damaging yaw angles. At the completion of shot 77, which was close to a success, the shield package was disassembled and the disrupter damage also evaluated. The presence of significantly large pieces of front shield debris caught in the disrupter was a cause for concern. This indicated that the front shield was possibly too thick, causing generation of potentially lethal debris. Looking at previous test results, these indicated that a thinner front plate would not effectively break up

the projectile. These two concerns and the results of shot 83 led to the decision to increase the thickness of the back plate. Consideration of the spread of the debris cloud as an indicator of shield success (refer to Figure 9) was the overriding factor in using one of the thicker front plates. The front plate thickness was slightly increased over the shot 77 configuration, even though shot 77 was classified as a near-success, to ensure success at a "worst case" yaw angle impact.

The resulting configuration was tested as shot 84 and was successful. Shot 85 repeated the results of shot 84, even with a significantly larger yaw angle. Figure 11 shows the close comparison of the damage profile in the disrupter. Each disrupter stackup contained numerous high-density pieces of front shield when disassembled, similar to shot 77.

The points discussed in the last several paragraphs are also shown by examination of flash x-ray data from shots 53, 55, 77, and 85. Figures 12, 13, 14, and 15 show the debris cloud flash x-ray

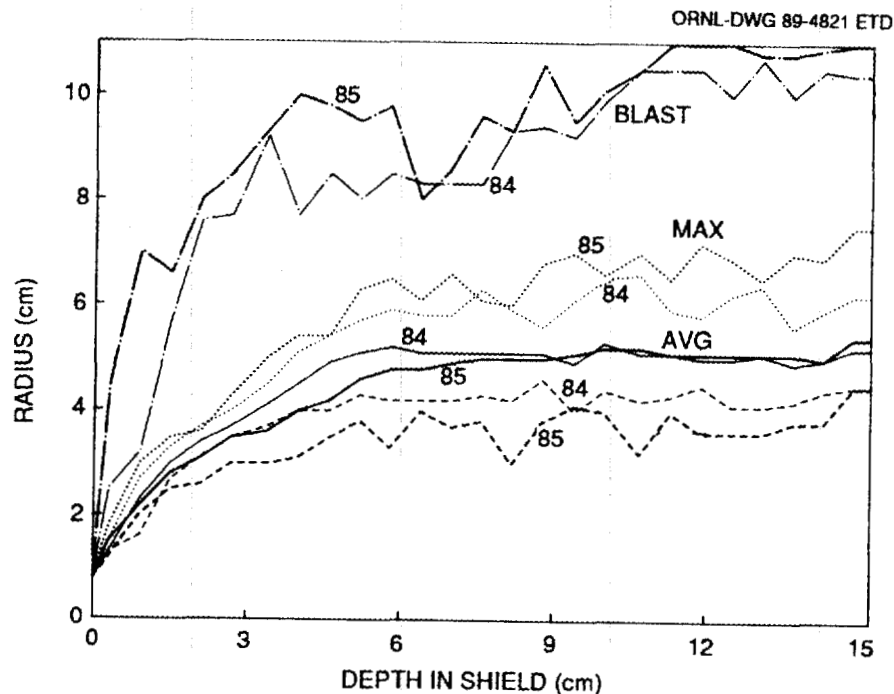
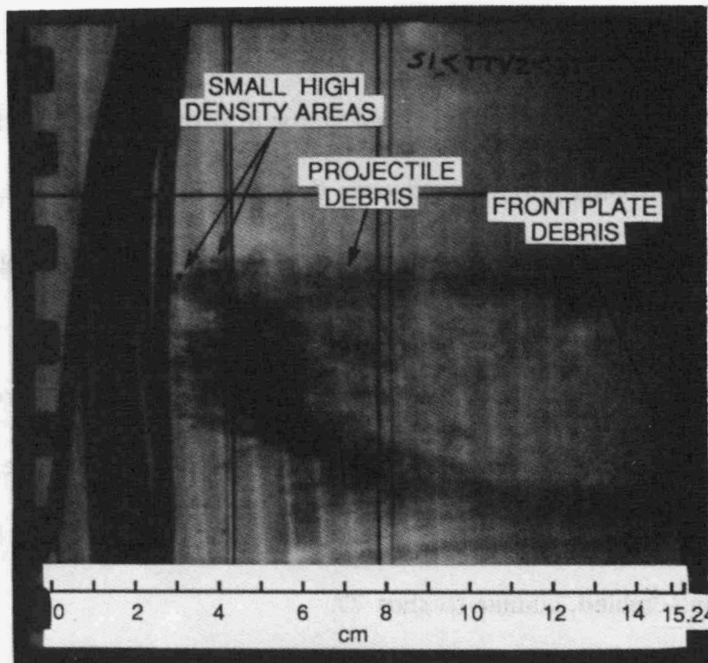
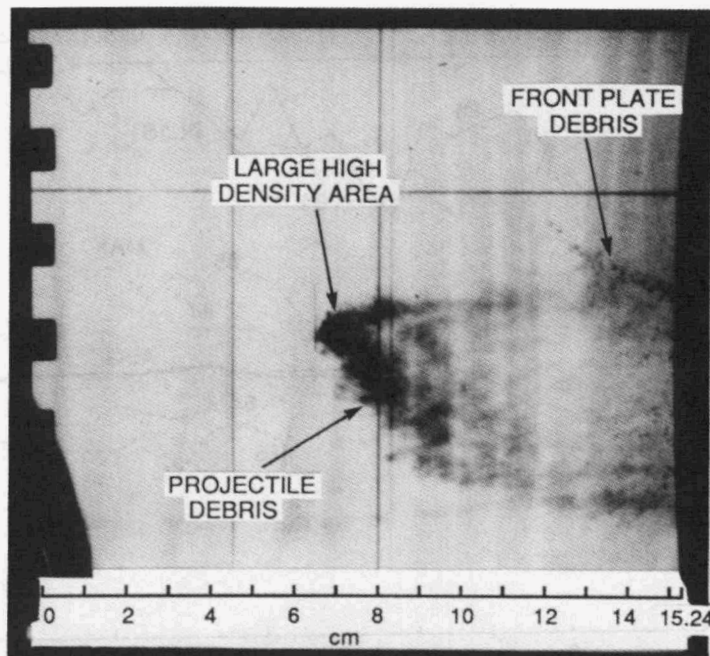


Figure 11. Disrupter damage comparison of shots 84 and 85

ORNL PHOTO 7119-89

Figure 12. Flash x-ray of shot 53 at 28 μ sec

ORNL PHOTO 7120-89

Figure 13. Flash x-ray of shot 55 at 28 μ sec

ORNL PHOTO 7121-89

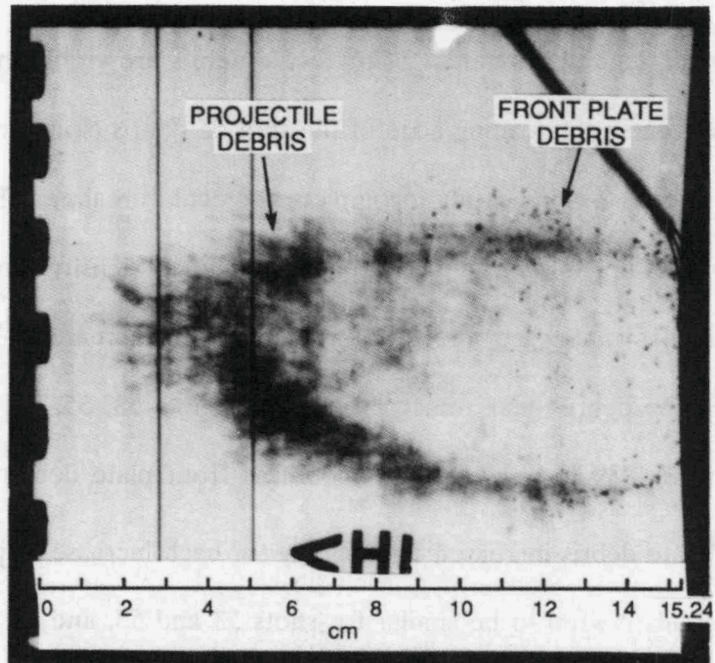


Figure 14. Flash x-ray of shot 77 at 31 μsec

ORNL PHOTO 7122-89

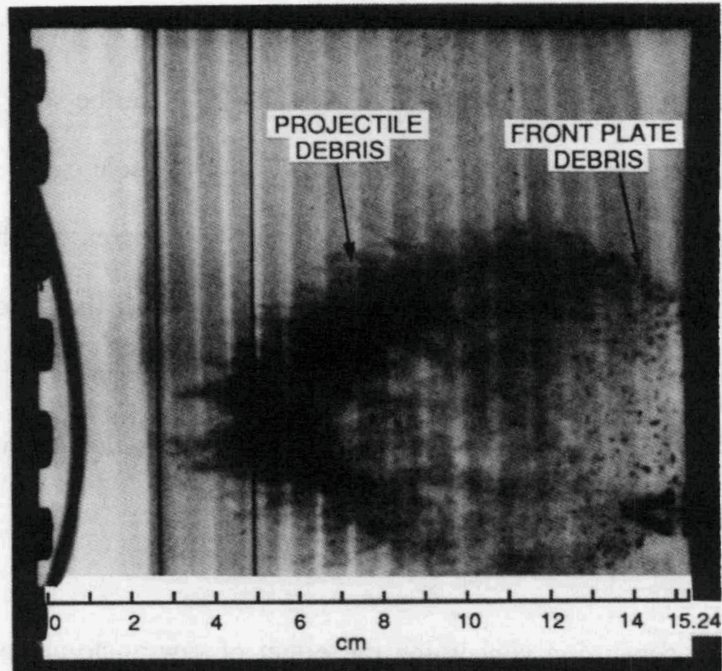


Figure 15. Flash x-ray of shot 85 at 31 μsec

taken of shots 53 (28 μsec), 55 (16 μsec), 77 (31 μsec), and 85 (31 μsec), respectively. For shot 53, only a very few, small, high density areas of projectile debris are visible in the leading edge of the debris cloud. However, in the leading edge of the shot 55 debris cloud, more and larger areas of high density debris are visible, indicating incomplete projectile breakup. The projectile in shots 77 and 85 was well broken up, as seen by the smooth, evenly low density projectile debris clouds. As the front plate thickness increased, the resulting debris also increased. This can be seen by successively comparing the debris near the front plate for shots 53, 55, 77, and 85, in order of increasing plate thickness. While only a small amount of front plate debris is visible in shot 53 (Figure 12), the front plate debris increased significantly for each increase in plate thickness. The spread of the debris clouds is seen to be similar for shots 53 and 55, and for shots 77 and 85, by comparing Figure 12 with 13 and Figure 14 with 15. Further comparison of the clouds for shots 53 and 55 with those for 77 and 85 shows the much greater spread of the latter two. While this phenomenon was seen before in the disrupter blast profiles of Figure 9, the disrupter blast profiles only reveal the damage spread, not whether the damage was caused by projectile debris or by front plate debris. From the flash x-ray data of Figures 14 and 15, it can be seen that, while the front plate debris had increased and spread out more, this was not the sole cause of the wider damage profile. The projectile debris has also spread over a much wider area for shots 77 and 85. The final information shown in the flash x-ray data of Figures 12-15 is the time after impact versus travel through the disrupter material. This was shown earlier in Figure 10. The data for Figure 10 were obtained from all available flash x-ray data, so the debris clouds shown in Figures 12-15 are actually four of the data points for Figure 10.

Results other than the conclusion concerning the effect of yaw angle are also of interest. The fifteen holes resulting from testing cover a range of front plate thicknesses. For each shot, the

ratio of plate thickness to projectile diameter and of average hole diameter to projectile diameter was calculated. These results are given in Table 4 in numerical form. The same results are shown graphically in Figure 16. Also graphed in Figure 16 is the early section of a plot of D/d versus t/d (D = average hole diameter; d = projectile diameter; t = plate thickness) from Bjork for aluminum impacting on aluminum at 7 km/s. Comparison of the data points available for stainless steel on stainless steel to the line given for aluminum on aluminum indicates that a similar but not identical line exists for stainless steel. The data point for shot 66 is shown, although it is a hybrid consisting of stainless steel on aluminum. The fifteen data points available here do not provide a complete line comparable to Bjork's, being confined to the thin plate region, and do not conclusively prove that the impact of stainless on aluminum (shot 66) is a different curve also. However, the data do indicate that (1) aluminum on aluminum is different from stainless on

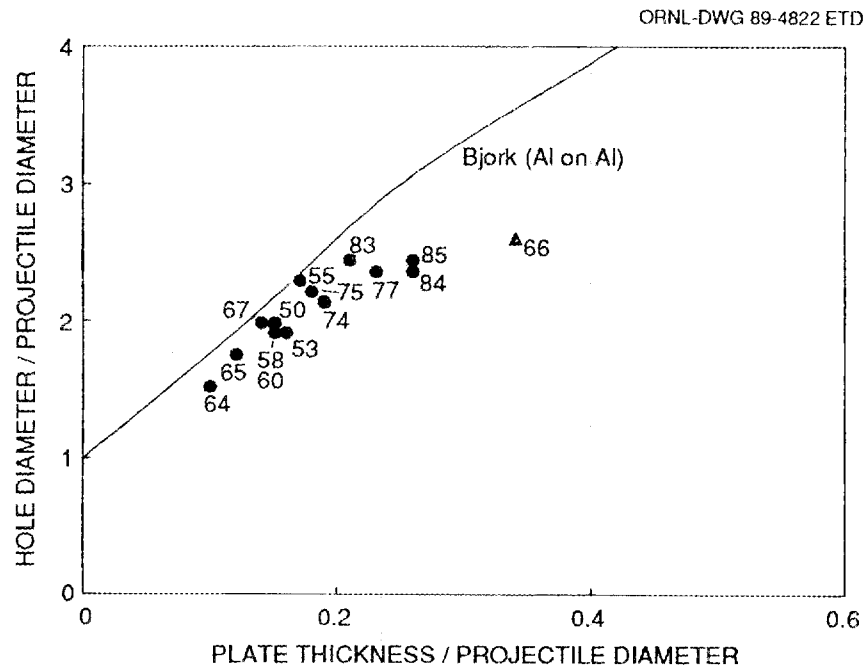


Figure 16. Front hole size versus plate thickness

stainless with regard to the hole size generated and (2) caution should be exercised in applying such curves to the impact phenomena of differing metals.

Another phenomenon indicated by the front plate holes of these tests (refer again to Table 4 and Figure 3) is an apparent correspondence between thicker front plates and a smoothing out of the effects of yaw angle on front plate hole shape. This is shown in Table 6, a rearrangement of Table 4. The data is listed in order of increasing difference between maximum and minimum hole diameters. Considering the differences in impact yaw angle, the thicker plates tend to have less elliptical front hole damage than the thin plates do from yawed impacts. There is really not enough data to conclusively prove or disprove this effect, but it is of interest, particularly if the same lessening of yaw effect could be seen in the debris generated by impact.

Comparison of shots 65 and 66 is also of interest, in that the two were of identical areal density but used stainless steel (65) and aluminum (66) front plates of different thickness. There are notable differences in the test results. First, from Figure 3 and Figure 16, it is obvious that the front holes produced by impact varied significantly in size. Also, the blast damage in the disrupters was different. This is shown in Figure 17. The blast damage for shot 66 started out as a wider damage spread, but as the penetration through the disrupter increased, the spread for 66 did not continue this way, finishing up as significantly less spread out. The yaw angles for the two shots were not noticeably different. Another difference between the two is that high-density sections of the front plate were found scattered through the disrupter for shot 66 but not in shot 65. With only two shots, this effect cannot be extensively analyzed. However, as previously mentioned, the test results are more clearly explained if thickness and material are considered separately rather than as areal density. This is evident for analysis of shots 65 and 66, since they are of equal areal

Table 6. Front plate results arranged in order of increasing ellipticity

Shot	t^a cm	D_{avg}^b cm	D_{max}^c cm	D_{min}^d cm	Area cm ²	D_{avg}^b /de	t^a/de	$\frac{D_{max}}{D_{min}}$
64	0.064	1.00	1.00	1.00	0.785	1.52	0.10	0.00
53	0.102	1.25	1.30	1.25	1.227	1.91	0.16	0.05
84	0.173	1.55	1.60	1.50	1.887	2.36	0.26	0.10
77	0.152	1.55	1.65	1.50	1.887	2.36	0.23	0.15
67	0.094	1.30	1.45	1.25	1.327	1.98	0.14	0.20
85	0.173	1.60	1.75	1.55	2.011	2.44	0.26	0.20
55	0.114	1.50	1.60	1.40	1.767	2.29	0.17	0.20
58	0.097	1.25	1.40	1.15	1.227	1.91	0.15	0.25
75	0.119	1.45	1.60	1.30	1.651	2.21	0.18	0.30
74	0.122	1.40	1.50	1.20	1.539	2.13	0.19	0.30
50	0.097	1.30	1.50	1.15	1.327	1.98	0.15	0.35
65	0.076	1.15	1.40	1.00	1.039	1.75	0.12	0.40
60	0.099	1.25	1.50	1.10	1.227	1.91	0.15	0.40
66	0.224	1.70	1.90	1.50	2.270	2.59	0.34	0.40
83	0.139	1.60	1.80	1.40	2.011	2.44	0.21	0.40

a thickness

b average hole diameter

c maximum hole diameter

d minimum projectile diameter

e projectile diameter

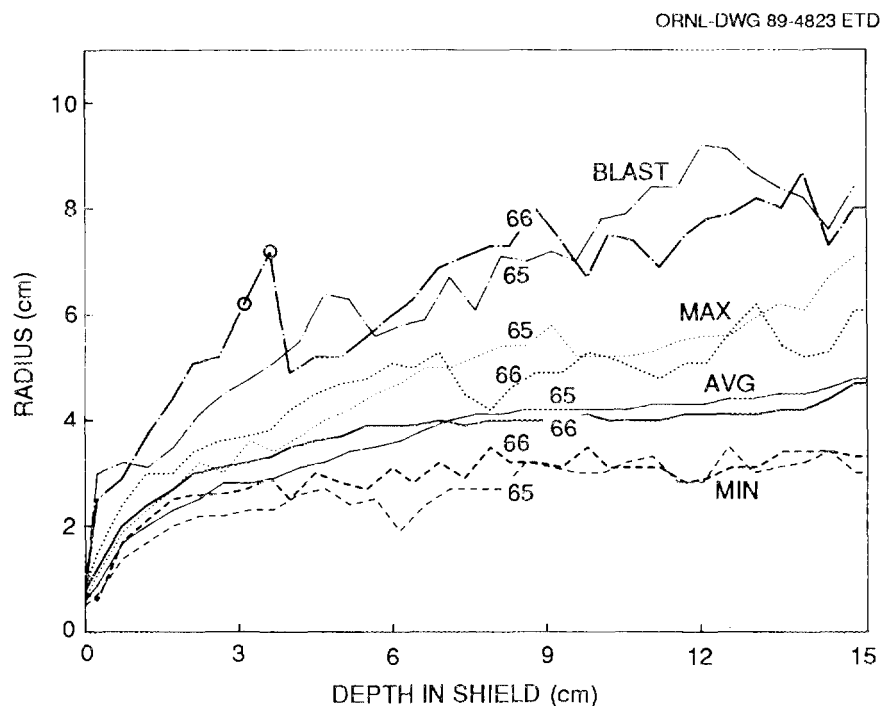


Figure 17. Disrupter damage comparison of shots 65 and 66

density and their differences are not due to yaw effects. The presence of front plate material in the disrupter indicates the plate is too thick, which does not also necessarily indicate the projectile has been completely broken up. The back plates for 65 and 66 indicate incomplete projectile breakup, as do the disrupter profiles. Thus the front plate for shot 66 is simultaneously "too thick" and "too thin," due to the material differences between aluminum and stainless steel. The results from these two shots are of interest in the consideration of shield literature on other research (Swift and Hopkins, 1970), which indicate material is not important as long as the areal density is the same for two front shields.

Shot 83 is briefly discussed here due to a slight difference in shield configuration. The front plate for this shot was composed of two layers of 21-6-9 stainless steel, each 0.070 cm thick, rather than a single layer of thickness 0.140 cm. The total thickness of the two layers falls between the 0.152 cm front of shot 77 and the 0.114 cm of shot 55. Resulting damage profiles in the disrupter layers

of these three shots are compared in Figure 18. No difference in the spread of debris was generated other than that due to the change in plate thickness alone, as the damage for shot 83 falls between that of shot 55 and shot 77, as would be expected. Having two layers rather than one homogeneous layer did not appear to produce either an increase or decrease in projectile breakup.

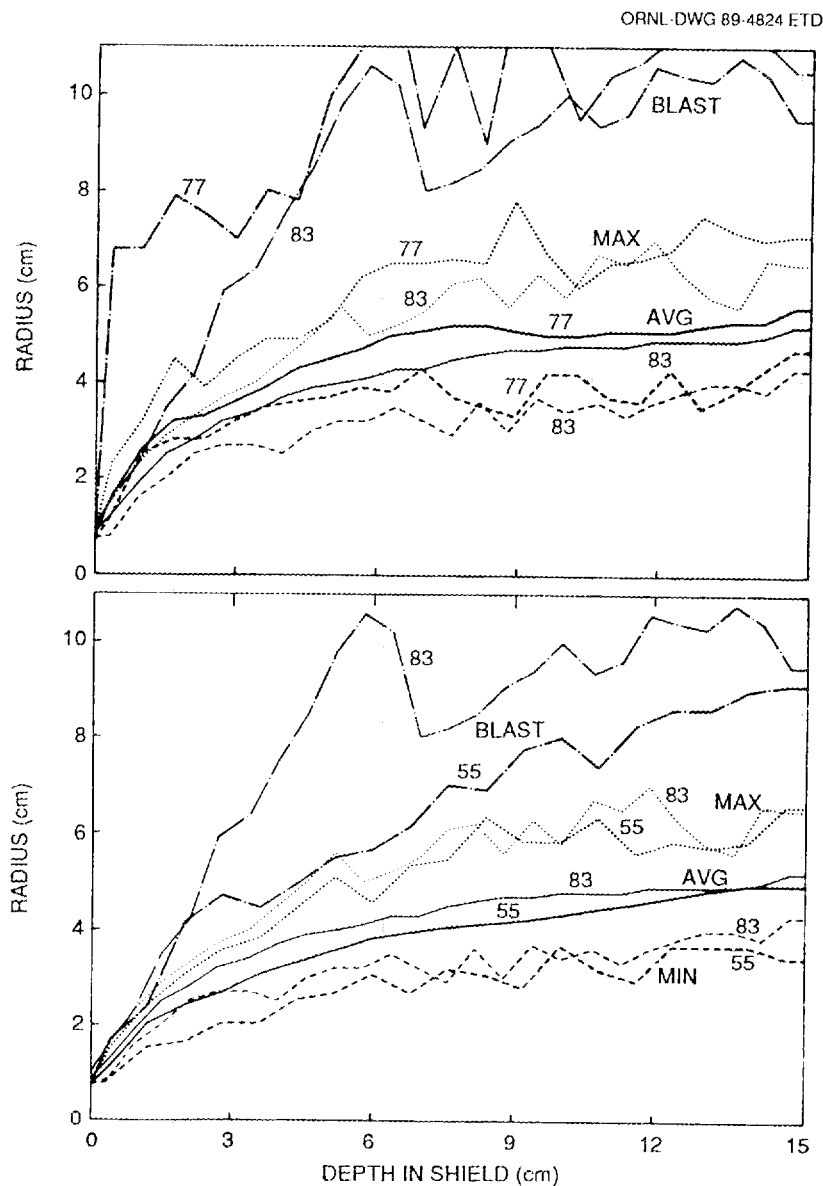


Figure 18. Disrupter damage comparison of shot 83 with 55 and 77

Another area of discussion from the results of the stainless steel testing is the possibility that stainless steel is a more damaging, harder to break up projectile than can be attributed to its density alone. The damage inflicted by the stainless steel projectiles was more severe than predicted for layered shields but not for the homogenous solid aluminum shield. The amount of energy in the projectile was not unexpected; the difficulty encountered in obtaining enough projectile breakup for a successful shield was unexpected.

Effective layered shields designed for the lexan, aluminum, and tantalum-tungsten threats provided more satisfactory projectile breakup than shields designed using similar design parameters for the stainless steel threat. Specific examples illustrating this point are: (1) shot 41, aluminum projectile and front plate, plate thickness to projectile diameter ratio of 16.8%; (2) shot 54, tantalum tungsten projectile and stainless steel front plate, plate thickness to projectile diameter ratio of 21%, areal density ratio of 9%; and, (3) shot 84, stainless steel projectile and front plate, plate thickness to diameter ratio of 26.5%. These were all classified as successful shields and are the lowest overall weight obtained against their respective threats. The back plate of shot 41 was bulged overall but showed no sign of small bulges, thus indicating complete projectile breakup. This is a similar result to those obtained for the shields used against the lexan threat (ORNL Staff, 1989). The back plates for shields 54 and 84 both show small bulges superimposed on the larger bulge, indicating incomplete projectile breakup. However, the front plate for shot 84 is much thicker in relation to the projectile diameter than the front plate of shot 54. The stainless steel projectile was not completely broken up even with the higher plate to projectile ratios. At comparable ratios, the stainless steel shield back plates have numerous small holes rather than merely dents.

As a side note of consideration, the incomplete breakup of the projectile is of importance when considering the effect of yaw angle. If, due to projectile material/front plate/impact velocity combinations, the projectile is subject to borderline breakup, then yaw angle will be much more significant. If, as in the lexan shields, impact energy is such that the projectile is completely broken up or even vaporized, the yaw angle is insignificant. As previously noted, yaw angle was not a factor until the stainless steel shots. This leads back into the discussion of stainless steel lethality again.

Stainless steel should be expected to be harder to stop than lexan or aluminum due to its greater density. Limited data is available on impact velocities and pressures necessary for different materials, as given in Table 7 (a, b, c). Note that there are some inconsistencies in the data and also the very limited information available. The increase in lethality of stainless steel due to its increased density should be compensated by the plate thickness to projectile diameter ratio, assuming the front plate is also stainless steel. The further increase in damage potential of stainless steel projectiles, which is indicated by test results to date, could be attributable to some other property of the material. Stainless steel in its solid state has unique properties. It is known to be of high strength and heat resistance, to name just two. The behavior of the front shield and projectile, at and after impact, no longer can be described or modeled well by solid material properties. As indicated by the sketchy information in Table 7, other factors should be considered, particularly those related to changing state and properties of the resulting liquids. It is reasonable to assume that the unique properties of stainless steel as a solid might well correspond to significant liquid properties. As a simple example, water and syrup are both liquids, but hot syrup inflicts a great deal more damage and is certainly harder to clean up. Indications from available data are interesting but hardly conclusive.

Table 7a. Impact velocities/pressures required for projectile melt or vaporization

Material	Melting				Vaporization			
	Incipient		Complete		Incipient		Complete	
	Pressure Mb	A1 Impact Velocity km/s	Pressure Mb	A1 Impact Velocity km/s	Pressure Mb	A1 Impact Velocity km/s	Pressure Mb	A1 Impact Velocity km/s
Magnesium	0.48	5.40						
Aluminum	0.70	5.60	1.00	7.0	1.67	10.2	4.70	
	0.67	5.50	0.88	6.6				
	0.61	5.10	0.85	6.5				
Titanium	1.30	7.60						
Iron (steel)	1.80	7.90	2.10	8.80				
Cadmium	0.33	2.50	0.46	3.20	0.88	5.2	1.80	8.1
	0.40	3.0	0.59	3.9				
	0.33	2.5	0.43	3.15				
Copper	1.40	6.60	1.84	8.00	3.40	12.6	34.00	
	1.40	6.60	1.84	8.00				
Nickel	2.3	9.00						
Lead	0.25	2.00	0.35	2.60	0.84	4.8	2.30	9.1
	0.27	2.1	0.34	2.5				

Swift (1982)

Table 7b.

Material	Melting Temperature (°C)	Vaporization Temperature (°C)	Pressure to cause incipient melting (Mbar)	Pressure to cause complete melting (Mbar)	Pressure to cause vaporization (Mbar)
Aluminum	660	2057	0.6	0.9	-
Cadmium	321	767	0.4	0.46	0.8
Copper	1083	2336	1.4	>1.8	-
Gold	1083	2600	1.5	1.6	-
Iron	1535	3000	-	2.0	-
Lead	327	1620	0.3	0.35	1.0
Magnesium	651	1107	-	-	-
Nickel	1455	2900	>1.5	-	-
Titanium	1800	>3000	>1.0	-	-

Gehring (1970)

Table 7c.

Material	Melting		Vaporization	
	Incipient	Complete	Incipient	Complete
Rock	1.05	1.07	1.6	6.0
Aluminum	.67	.95	5.8	26
Steel	1.8	2.1	3.5	10
Cadmium	.33	.46	.7	5.3

Hart and Wessel (1986)

6. ANALYSIS METHODS

For impact and penetration at 7 km/s, very specialized analysis techniques are required. Since this impact velocity is above the sonic velocity in stainless steel (about 5 km/s), the presence of localized high intensity shock waves is a very important part of the overall impact phenomena. The analysis model must account for the shock wave phenomenon. For these impact conditions only the localized material response is important. The overall structural response is of secondary importance. This entire problem is characterized by submillisecond loading and response times, so that the integration step size must remain quite small and will thus preclude any significant structural response.

Very large displacement of these localized areas, including penetration and ejecta, requires that a hydrodynamic computer code or hydrocode be used. The hydrocode makes use of finite difference methods to approximate the solution of the governing partial differential equations. These equations are based on the conservation of mass, momentum, and energy, along with an equation of state and constitutive relationships to properly model the material behavior.

The Eulerian based version 120.2 of the Hull (Matuska and Osborn, 1987) hydrocode was chosen to model the projectile and front plate impact. The Eulerian version has a framework of cells fixed in space through which material flows. Consequently, very large deformations do not require a remesh or restart as in the Lagrangian or material fixed coordinate systems. The Hull computer code has been widely used in impact studies for a large range of velocities and for a variety of materials. Correlations with experimental data were good for the lexan projectiles studied in the first phase of this program as reported in the Fast Track Progress Report (ORNL Staff, 1989). Runs were performed using a CRAY XMP.

Material properties are the key parameters in the successful prediction of a hypervelocity impact event. (Stability criterion for the explicit integration scheme is also quite important.) For stainless steel the very high strain rate material properties are as well known as for most metals and much better quantified than nearly all nonmetals. The Mie-Grunieson material model was used to represent the projectile and the front plate. Appropriate values of ultimate strength and strain were used from tests at high strain rates. The disrupter material was modeled as a gas of appropriate density. This procedure has correlated well with experimental data in the past (ORNL Staff, 1989), since mass effects are the primary consideration.

Cell size and integration step size are also very important parameters for these high velocities. Integration step size is somewhat controlled by the internal code logic, but a stability factor is available to control the step size and make it consistent with the problem initial conditions and complexity. Thus the most important single parameter must be the cell size. Coarse meshes cause a filtering of the shock wave and will fail to give the resolution required locally at the contact points between the projectile and target. However, the tradeoff to using a very fine mesh involves the possibility of code execution problems (i.e., stalling) that can occur in very small cells with mixed materials.

In addition, the economics of running a fine mesh are also an important consideration. The economics of a three-dimensional problem are very important, since the three-dimensional problem is equivalent to running tens to hundreds of two-dimensional problems. Symmetry considerations are very important in two- and three-dimensional problems because the amount of storage and calculations can be reduced by factors of 2 or 4 by taking advantage of 1/2 or 1/4 symmetry. For the three-dimensional problems run here only half of the problem was modeled, taking advantage

of the symmetry about the center line. Even with the best efforts of using variable cell size, symmetry, and a minimum portion of the model, the requirements for storage of each time dump were very large. Calculations to 10 μ sec might typically have fifteen dumps and result in storage requirements of 90 to 100 x 10⁶ decimal words or about five extra long high density magnetic tapes containing 20 x 10⁶ words each. Retaining the results on the computer for postprocessing was a difficult problem because of these very large storage requirements. Consequently, the two-dimensional approximation was used when it was adequate, to give a picture of the phenomena important to the shield design.

7. ANALYSIS CONFIGURATIONS

The configurations chosen for analysis were very nearly identical to test conditions. A nominal value of 7 km/s was used for all analyses, to isolate all other phenomena. (Test values ranged from 6.738 to 6.975 km/s.) The models contained only the projectile, front plate, and enough disrupter to study the penetration and breakup of the projectile. The very thin front plate required that a small cell size (0.025 cm) be used in the penetration region of the problem. Consequently, the problems were very large if the back plate was included in the study. Table 8 lists a description of parameters for each problem number and an indication of the problem size by the total number of cells in the problem.

The first two problems (8.22 and 8.44) represent the three- and two-dimensional problems to evaluate the cylinder at 45 and 0 degree yaw impacts. Figure 19 gives the shield geometry with model boundaries for problem 8.22, the 45 degree yaw case. For the 0 degree yaw case, the two-dimensional analysis was adequate, and the configuration is shown in Figure 20. The spherical projectile of problem 8.54 was also included in the study as a baseline for comparison with the normal and yawed cylinder. With a constant mass the sphere diameter is slightly larger than the $L/D = 1$ cylinder, as can be seen by the parameters in Table 8. The problem geometry was the same as shown in Figure 20, with a sphere replacing the cylinder.

The three-dimensional analyses of problem 8.22 was so large that computational and storage costs soared. To continue this problem to 10 μ sec might have cost 10 to 20 CPU hours, so an alternative two-dimensional problem was begun to obtain an approximate solution for the yawed cylinder. In problem 8.64, shown in Figure 21, the projectile was modeled as a double cone with the side of the cone at 45 degrees to the front plate. From Table 8 it can be seen that the double

Table 8. Stainless steel projectile analysis summary

Problem number	Projectile		Plate Thickness t, cm	t/l	Velocity @ 2 μ sec	Velocity @ 10 μ sec	Number of cells	
	Shape	Dia. cm						Characteristic length, l
8.22*	Cyl	.66	.9334	0.10	.1071	6.23	N.A.	373464
8.44	Cyl	.66	.66	0.10	.1515	6.15	5.3	20475
8.54	Sphere	.75	.75	0.10	.1333	6.22	5.0	20475
8.64	Double 45° cone	.4737	.9747	0.10	.1026	6.8	6.1	22295
8.74	Double 45° cone	.4737	.9747	0.17	.1744	6.6	5.5	22295

*Three dimensional run.

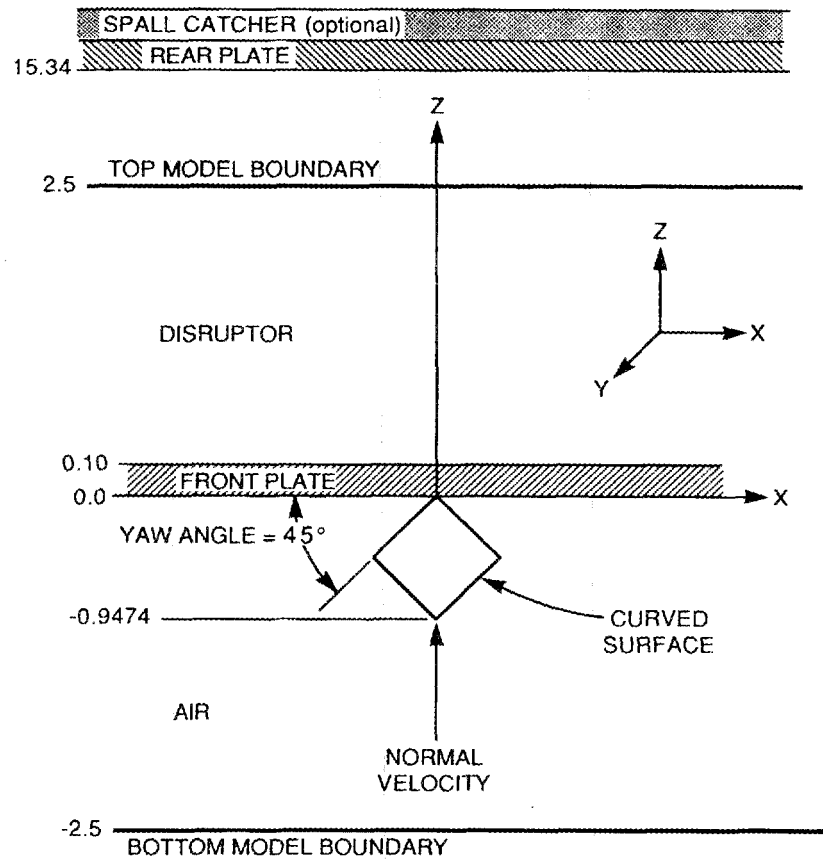


Figure 19. Problem 8.22 shield geometry with model boundaries

cone characteristic length is not significantly different from the cylinder with a yaw angle of 45 degrees. (0.9334 cm for the cylinder and 0.9747 for the double cone.) As will be discussed later, the projectile debris patterns at 2 μsec are very similar for these two configurations, so the less expensive two-dimensional analysis was run to 10 μsec . Problem 8.74 duplicates 8.64, except that the front plate thickness was increased from 0.1 cm to 0.1727 cm to correspond with the values used in tests 84 and 85.

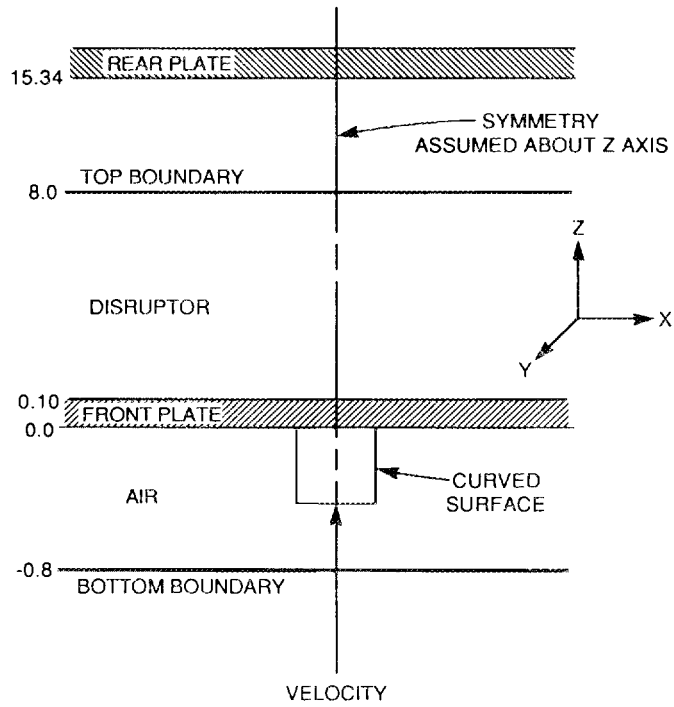


Figure 20. Problem 8.44 shield geometry with model boundaries

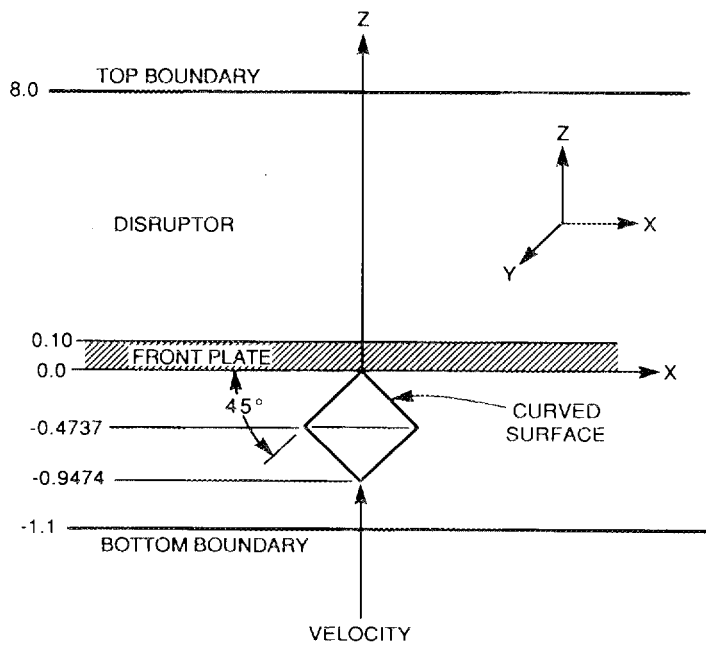


Figure 21. Problem 8.64 shield geometry with model boundaries

8. ANALYSIS RESULTS

8.1 Comparison of Normal and Yawed Cylinder

Density plots for the projectile, front plate, and disrupter are shown in Figure 22 as the penetration has been nearly completed for the normal impact and about 1/2 complete for the yawed projectile. These plots were included to provide a scaled picture of the two configurations. However, to visualize the shocked material in the projectile, the projectile alone will be shown in the remainder of the figures.

The sequence of projectile density plots in Figure 23 shows the compression shock wave upon initiation at 0.4 μsec and the progression of the wave at 0.8, 1.0, and 1.2 μsec . The dark area near the nose of each projectile plot represents a density increase from 7.86 to some value greater than 8 g/cm^2 . As the compression shock wave travels to the rear of the projectile, the geometric shape of the projectile greatly affects the shape of the shock wave, as noted in the frames for 0.8 and 1.0 μsec . By the very short elapsed time of 1.2 μsec the compression wave has reflected from the rear surface of the projectile, becoming a very strong tensile wave that has caused considerable erosion on the aft portion of both projectiles. The primary difference in the last frames of Figure 23 is the low density region that has formed in the nose of the normal impact case, whereas the yawed cylinder appears to be at the nominal density (i.e., $>7.5 \text{ g/cm}^2$) for the forward portion of the projectile.

The continuation of the projectile erosion and breakup at 2 μsec is shown in Figure 24. Here the yawed projectile nose has remained relatively intact, while the normal impact projectile has very low density regions that cover nearly the entire nose section of the projectile. This is an early indication that the projectile breakup will be more complete for the normal impact than for the yawed impact.

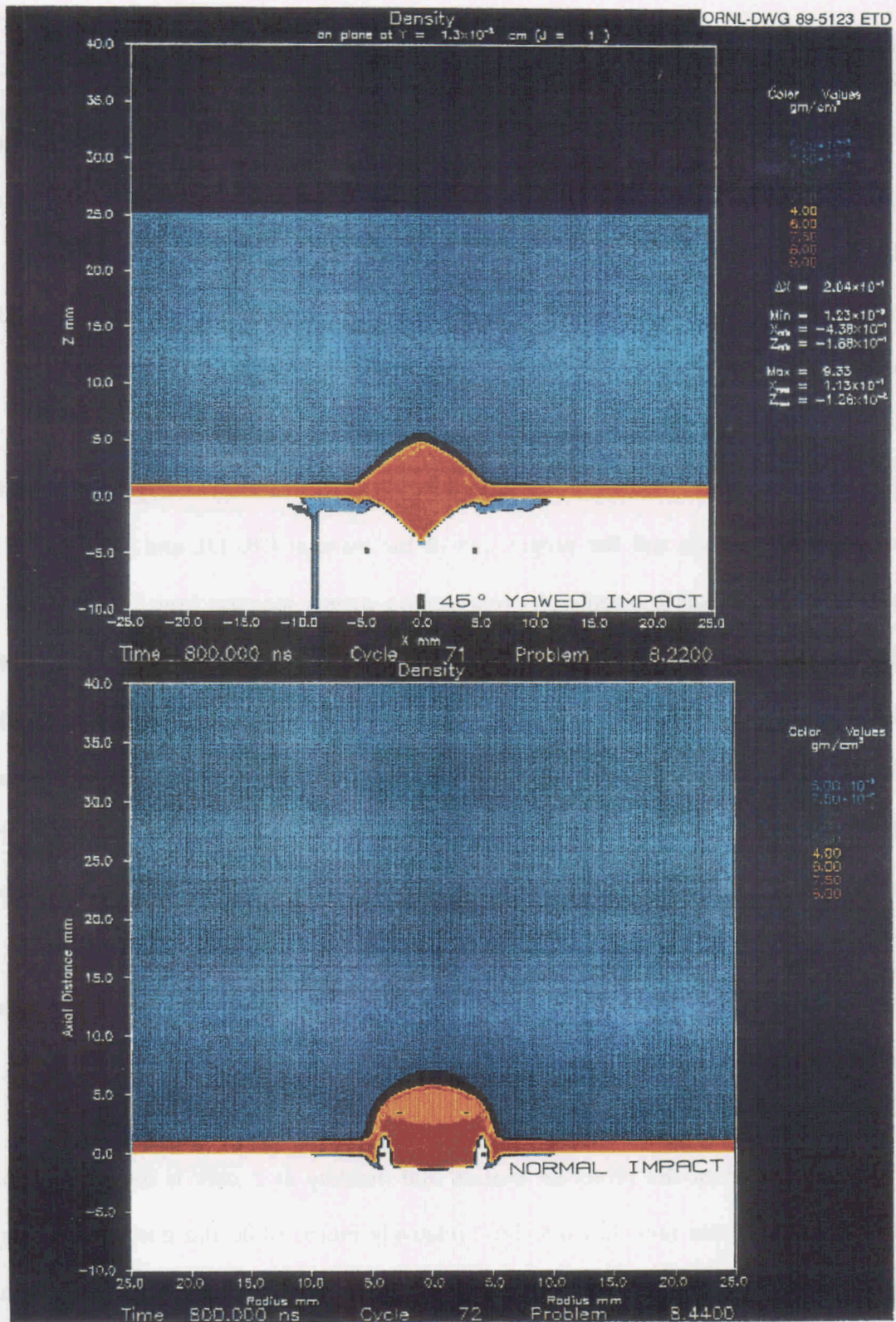


Figure 22. Density plots of total shield model (8.22 and 8.44) at 0.8 μ sec.

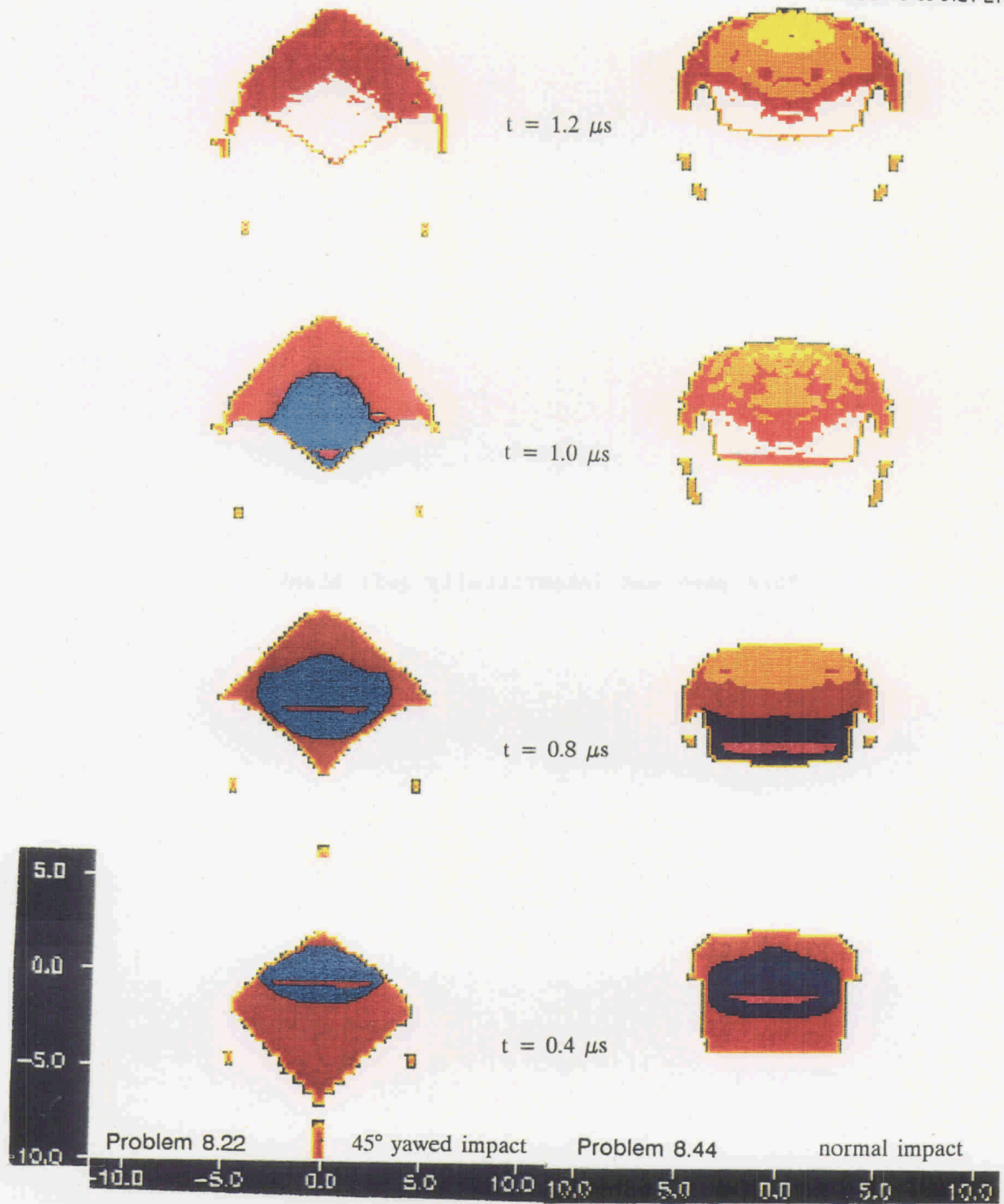


Figure 23. Projectile density profiles to show shock wave progression during front plate penetration

This page was intentionally left blank

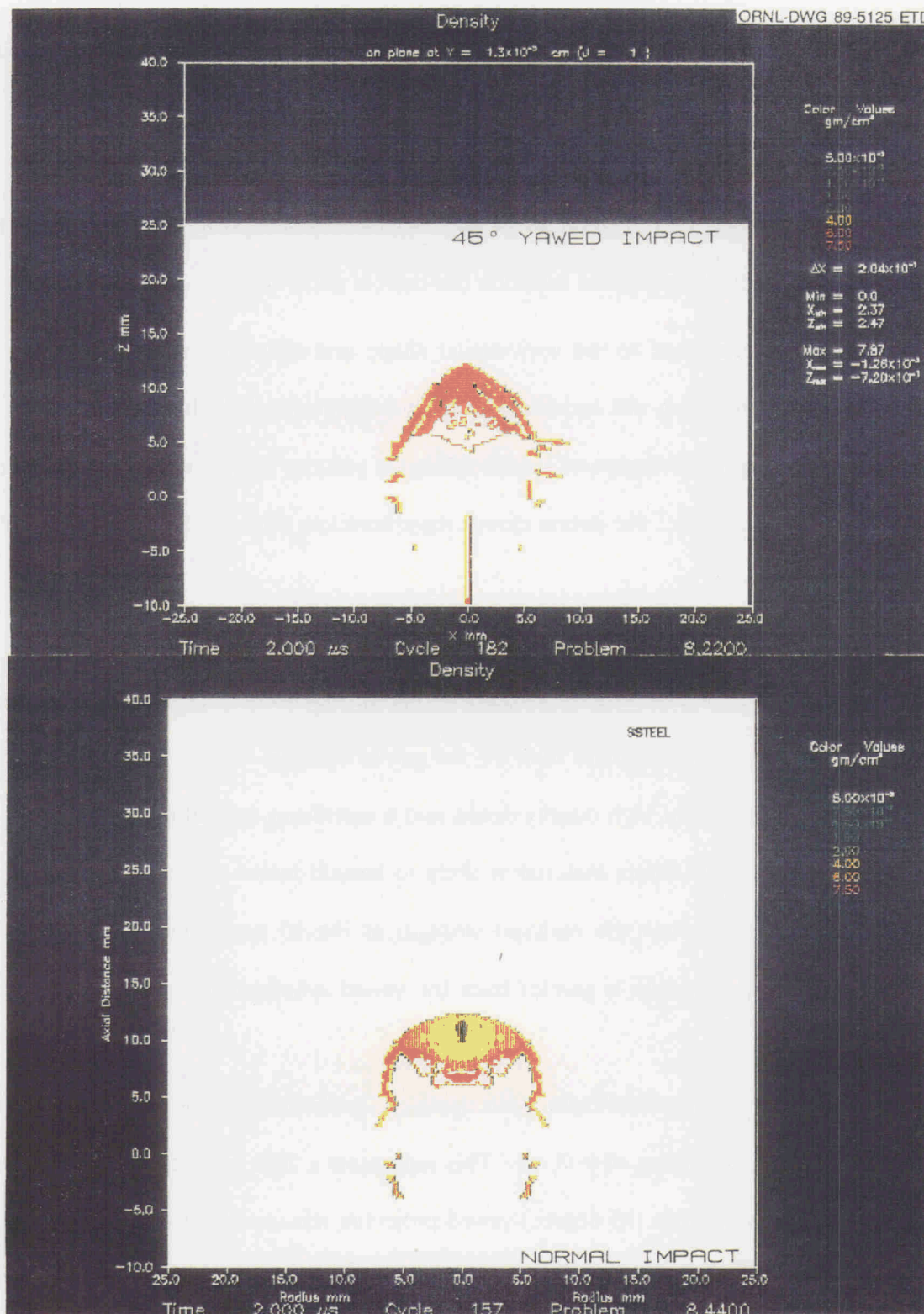


Figure 24. Projectile density profiles to compare normal and yawed impact at 2 μsec.

It was desirable to continue the analysis until a more complete pattern of breakup was achieved. To continue the three-dimensional analysis was prohibitively expensive due to problem size and the small time steps required for stability. The two-dimensional double cone problem resulted in a good approximation to the three-dimensional yawed cylinder, as shown in Figure 25. In each case the nose of the projectile debris remained intact with much of the aft portion eroded away at the 2 μsec time point. The good agreement between the double cone and the yawed cylinder results at 2 μsec can likely be attributed to the very similar shape and characteristic length of the two projectiles. Since the correlation was satisfactory, the two-dimensional double cone problem was continued to 10 μsec . Figure 26 compares the double cone and the normal impact cylinder debris clouds at 10 μsec . At this time, the debris clouds have traveled about 6 cm or almost half the distance to the rear plate.

The results at 10 μsec reinforce the early indication that the projectile breakup for the normal impact cylinder was much more complete than for the yawed cylinder. The yawed cylinder debris cloud still contains a thin shell of high density debris and a significant central cone-shaped section of high density material. This debris material is likely to remain intact, since the stresses in the problem have dropped well below the material strength at the 10 μsec time point. Thus the likelihood of back plate penetration is greater from the yawed cylinder debris cloud.

To investigate the effects of increased front plate thickness, problem 8.74 was run using the plate thickness of tests 84 and 85, a value of 0.17 cm. This represents a 70% increase over the previous tests and analyses. The worst case (45 degree) yawed projectile was used for this problem, and the longer projectile characteristic length and the thicker front plate caused complete penetration to occur somewhat later than in the previous analyses. However, the compression shock wave in the

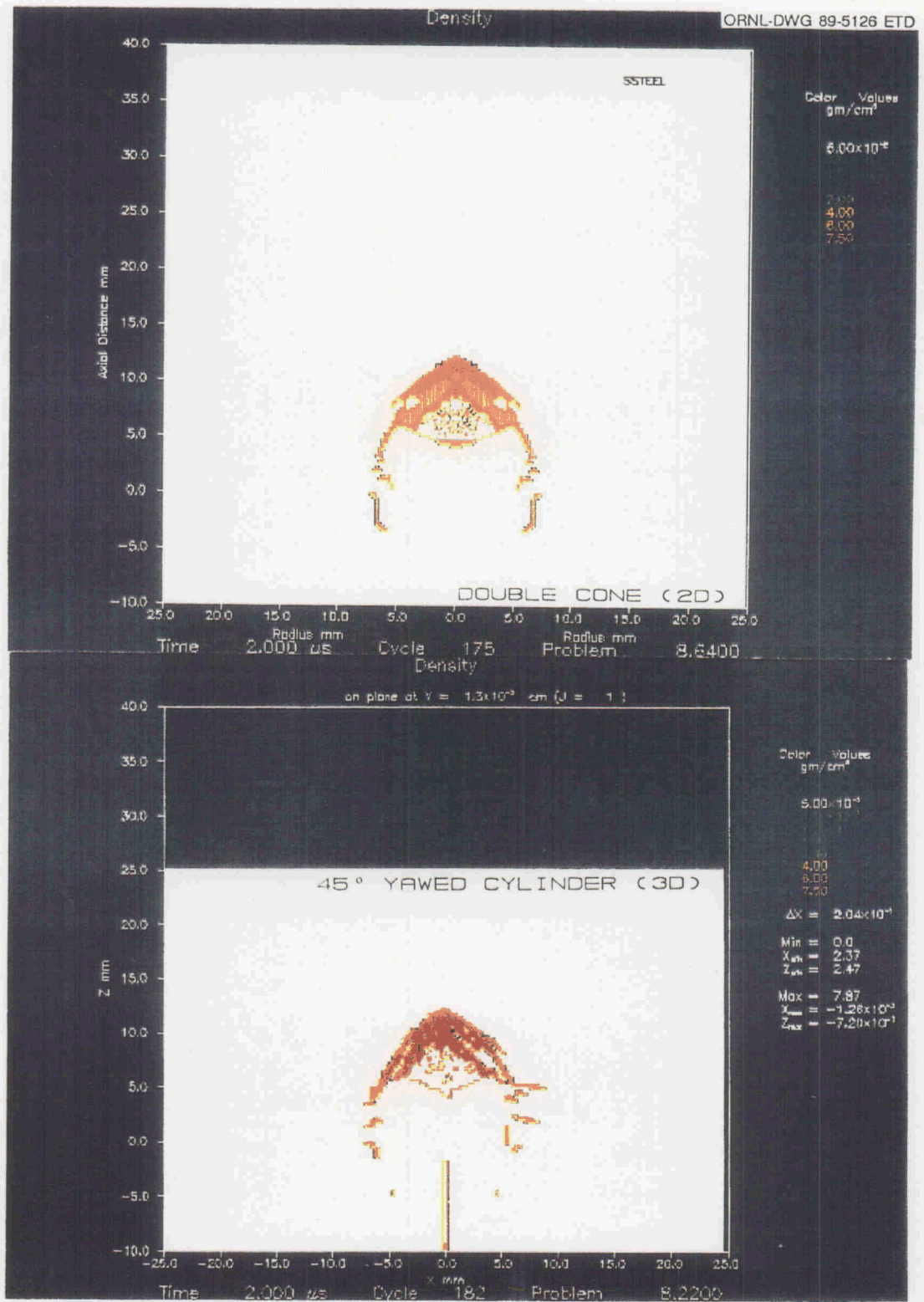


Figure 25. Projectile profiles to compare double cone (2D) to the yawed cylinder (3D) at 2 μsec.

This page was intentionally left blank

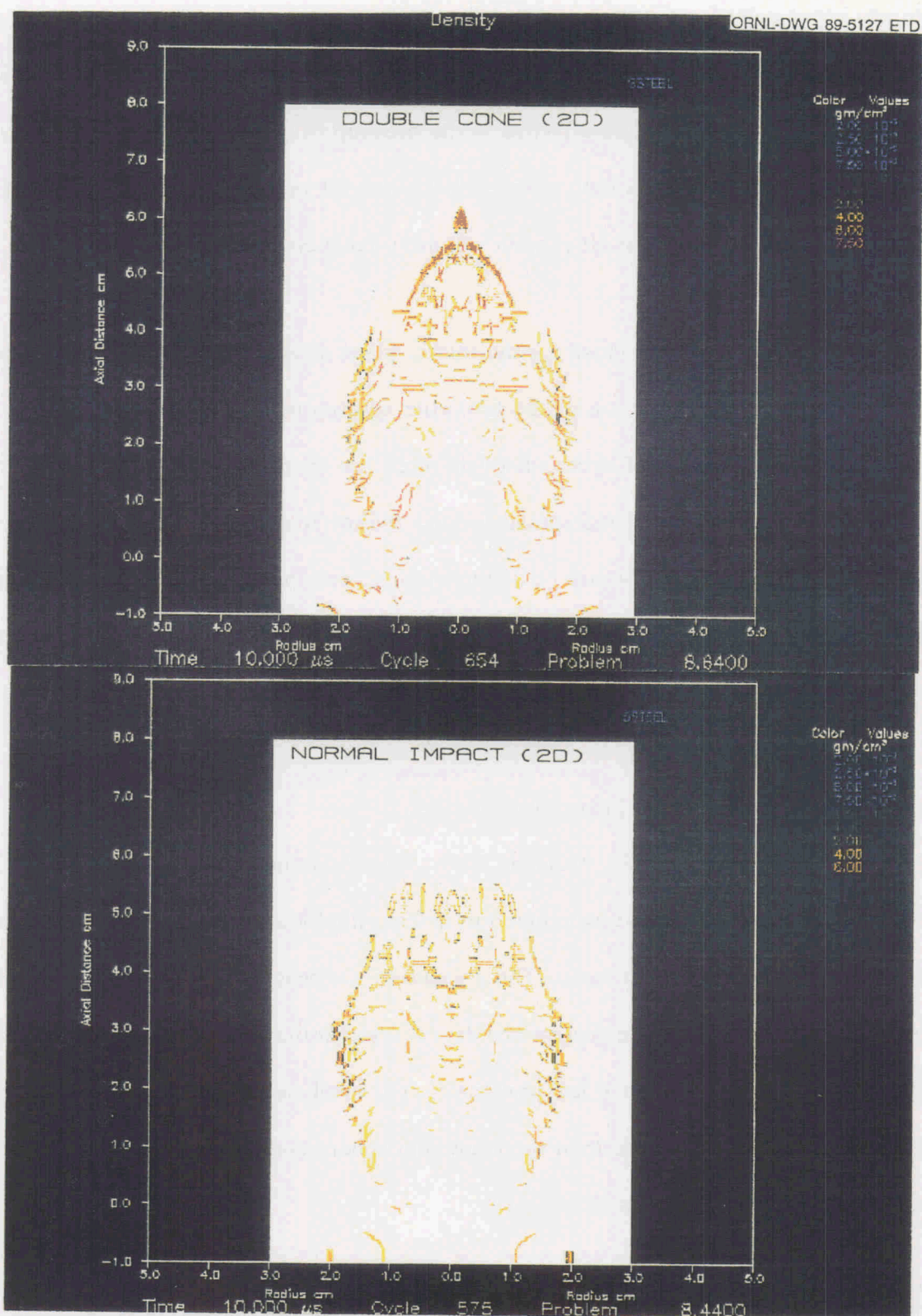


Figure 26. Projectile density profile at 10 μ sec; comparison of double cone and normal incidence cylinder

projectile was very similar for the thick and thin front plates, as seen by comparing problems 8.64 and 8.74. Figure 27 shows these results at 2 μsec in time near the end of penetration. The thicker plate of problem 8.74 has been more effective in the breakup of the projectile nose. At 2 μsec the thick plate of problem 8.74 has not yet eroded away the aft portion of the projectile, but the pressures are still very high and the aft portion will most likely be eroded.

At 10 μsec after impact the debris cloud for the thicker plate, shown in Figure 28, was somewhat of a surprise. A small central portion of the projectile appears to be still intact. However, the density plots show that the shell of debris aft of the nose has been much better dispersed. Also visible is the much wider debris cloud spread for the thicker front plate. The single nose tip projectile remaining in problem 8.74 may be due to the inherent symmetry of the two-dimensional problem that might not exist in the three-dimensional case of the yawed projectile. The comparison at 10 μsec shows considerable improvement in debris breakup for the thick front plate case.

8.2 Comparison of Cylindrical and Spherical Projectiles

Several references (Morrison, 1972; Maiden, 1965; and Piekutowski, 1987) were found that suggested a greater shield thickness was required to defeat cylindrical projectiles than was required for spherical projectiles of the same mass. This conclusion was reached for cylinders with $L/D = 1$ and impact at low yaw angles. The analysis and data covered in this report are in agreement with this conclusion, noting the qualifier of low yaw angle. The ideal case of a completely orthogonal impact appears to be less destructive than the equivalent sphere and considerably less destructive than the cylinder at a 45 degree yawed impact.

Figure 29 compares the spherical projectile (problem 8.54) with the ideal case of 0 degree yaw for the cylinder. Results are shown at 2 μsec into the thin front plate ($t = 0.1$ cm), the same

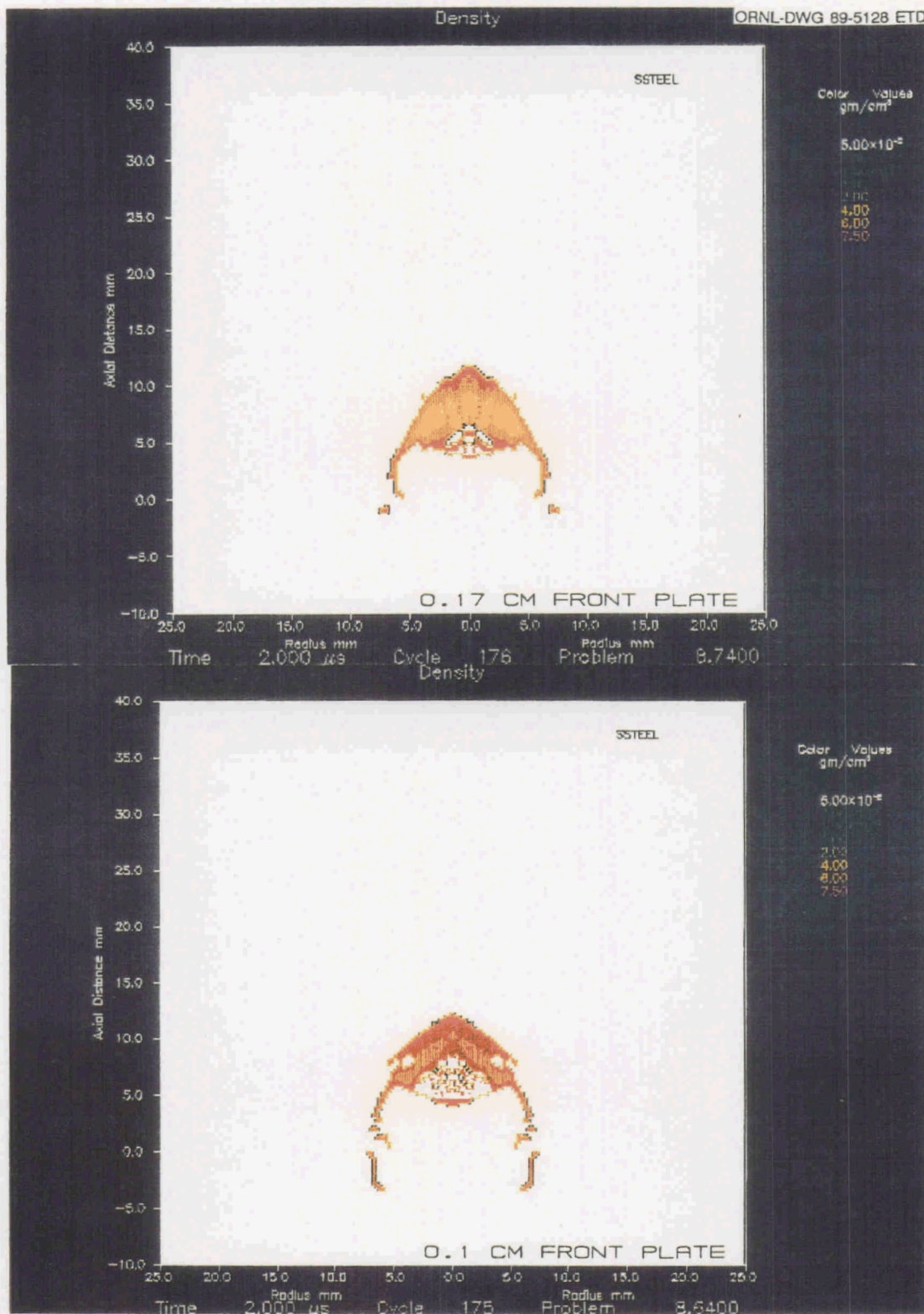


Figure 27. Projectile density profiles at 2 μsec; comparison of double cone debris cloud versus front plate thickness

This page was intentionally left blank

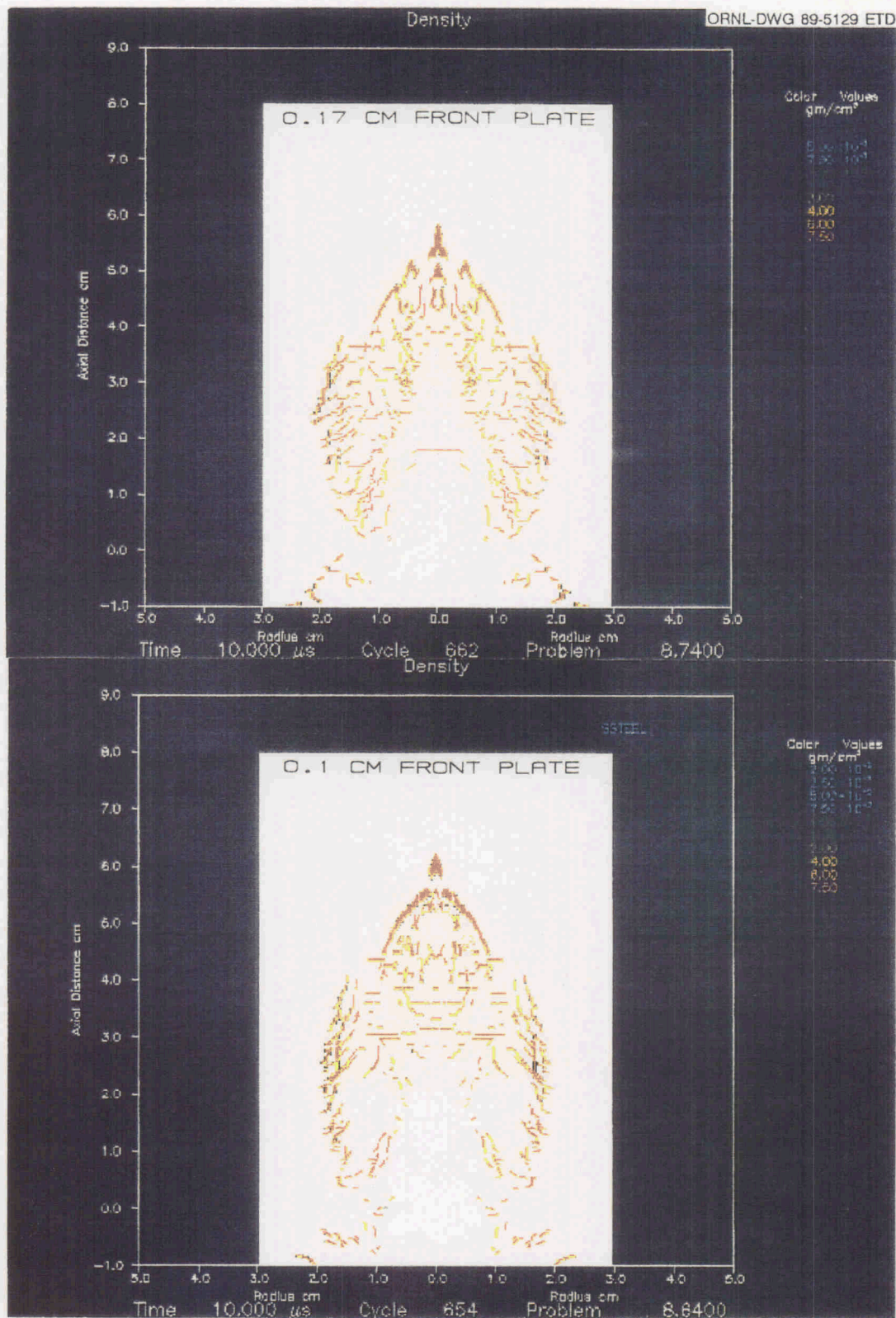


Figure 28. Projectile density profiles at 10 μ sec; comparison of double cone debris cloud versus front plate thickness

This page was intentionally left blank

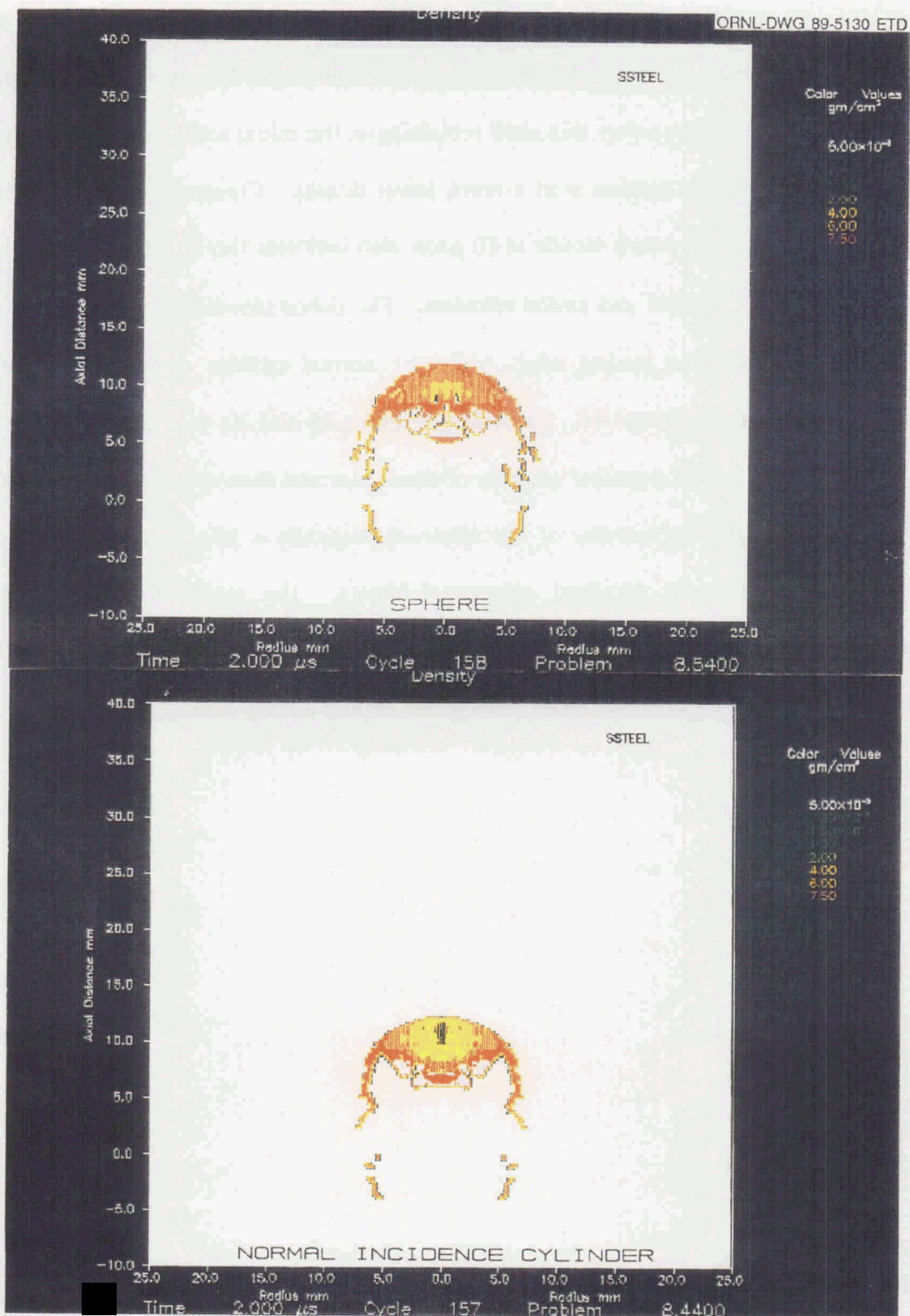


Figure 29. Comparison of sphere and normally incident cylinder debris clouds at 2 μsec

plate configuration as shown in Figure 25. The density contours of the two figures indicate that the lethality of the sphere is intermediate to the normal and yawed cylinders. The leading edge of the spherical projectile has a very thin shell remaining at the initial stainless steel density, while much of the aft and central portion is at a much lower density. Comparison of Figure 30 with Figure 26, both showing the debris clouds at 10 μ sec, also indicates the lethality of the sphere to fall between that of the normal and yawed cylinders. The debris cloud for the sphere has dense clusters of material near the leading edge, while the normal cylinder debris cloud is entirely composed of reduced density material. Comparing Figures 26 and 30, it is clear that the yawed cylinder debris cloud contains a greater quantity of dense material than the cloud for the spherical projectile. Consequently, the lethality of the spherical projectile is less than that of the yawed cylinder but greater than the idealized orthogonal impact. The reason for the test data to consistently show the cylinder to be more lethal than the sphere lies in the extremely low probability for the occurrence of the exact orthogonal impact during testing.

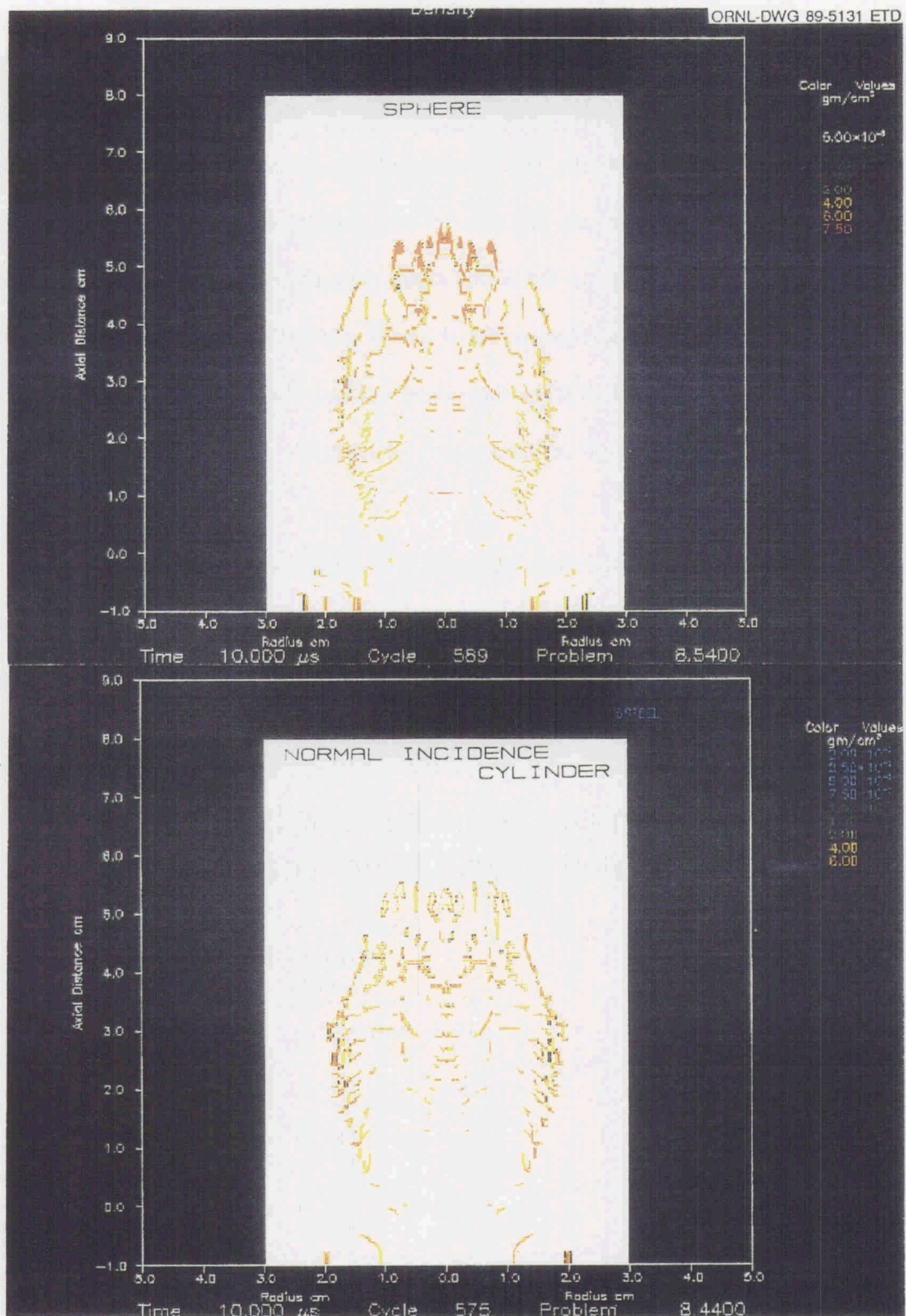


Figure 30. Comparison of sphere and normally incident cylinder debris clouds at 10 μ sec

9. COMPARISON OF ANALYTICAL AND TEST RESULTS

From the test results as discussed earlier, an orthogonal hit was shown to be less damaging than a yawed impact. This is indicated by the comparison of shots 53 and 67, primarily, but also by the survival of the witness plate for shot 64. These test results correlate very well with the analytical work, as the orthogonal impact case was the least lethal of the three cases studied. The greater amount of low density material shown in the debris cloud from the orthogonal impact, referring to Figure 26, matches well with the lesser damage for the back plate of shot 53. Correspondingly, the high density material left in the debris from the yawed impact, also shown in Figure 26, gives a good prediction of the gross failure of the back plate for shot 67.

Analytical results also correspond well with the test results for front plate hole diameters. The calculated and analytical values for applicable cases are compared in Table 9. Major and minor ellipse axis values are given for the analytical front plate results. These are compared to the

Table 9. Comparison of analytical and experimental front hole diameters

Shot Number	Front hole diameter max - min, cm	
	experimental	analytical
50 t = 0.097 cm	1.50 - 1.15	1.50 - 1.17
53 "	1.30 - 1.25	1.17 - 1.17
58 "	1.40 - 1.15	1.50 - 1.17
60 "	1.50 - 1.10	1.50 - 1.17
67 t = 0.173 cm	1.45 - 1.25	1.50 - 1.17
84 "	1.60 - 1.50	1.62 - *
85 "	1.75 - 1.55	1.62 - •

*Not calculated due to two-dimensional analysis

maximum and minimum diameters measured from the front plate holes, for the cases having appropriate front plate thicknesses.

Figure 31 includes analytical results for front plate debris, both problem 8.64 and 8.74, at 10 μ sec after impact. Comparison of the two shows no significant difference in the spread of the debris for the thin plate of problem 8.64 and the thick plate of problem 8.74. Referring to Figure 28, no difference in the spread of projectile debris for the two problems can be seen also. This does not agree with the marked difference in damage spread due to plate thickness seen in the experimental results (Figures 4 and 9) and previously discussed. This discrepancy might be resolved by extending run times.

In the earlier discussion of the test results, shots 66, 77, 84, and 85 were mentioned as having significant pieces of front plate debris in the disrupter layers when disassembled. These are the thickest front plates tested. To compare this phenomenon with analytical results, the 0.17 cm front plate, as used in problem 8.74, is applicable. Examination of the plot of the front plate debris of problem 8.74, referring to Figure 31 again, shows the presence of high density material in the cloud. High density front plate material can be clearly seen in the flash x-ray for shot 85 (Figure 15). Also visible in Figure 31 is the presence of considerable front plate ejecta, traveling away rather than into the shield. The thicker front plates, especially those for shots 84 and 85, show a very definite ragged lip around the rim of the hole. This indicates a large amount of outward ejecta.

There were no detectable pieces of front plate in the disrupter material when shot 67 was disassembled. Comparing the analytical results from problem 8.74 and for problem 8.64, shown in Figure 31, the debris from the thinner plate is overall of lower density with fewer and smaller high

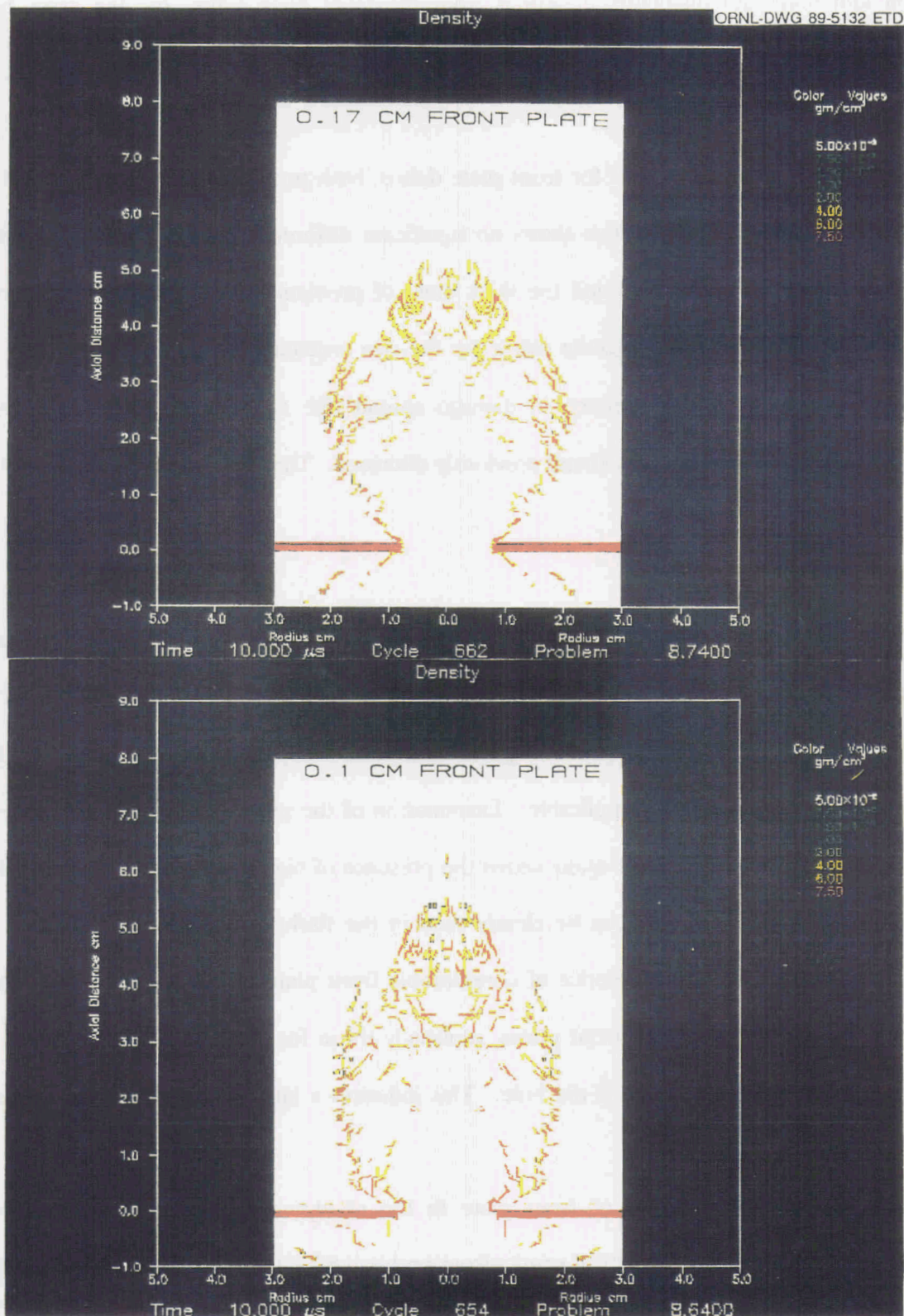


Figure 31. Front plate debris for problems 8.74 and 8.64 at 10 μ sec.

density patches visible. This corresponds well with the experimental results, as seen in Figures 12 and 13, the flash x-ray data for the thinner front plates. The lesser amount of front plate ejecta shown in the analysis for the thinner plate matches the holes seen in the thinner front plates tested, which each have a much smaller and less ragged damage lip on the rims.

Along with the analysis problem numbers and parameters used for each, Table 8 includes the debris cloud velocities calculated for each case at 2 and 10 μsec . These results correspond well with measured debris cloud travel times. Figure 10, which shows debris cloud position versus time as measured from flash x-ray data, indicates the debris cloud for shot 53 had slowed significantly more than those shots with equal thickness front plates, such as shot 67. From Table 8, using problem 8.44 to model shot 53 and problem 8.64 to model shot 67, this trend is accurately predicted.

Calculated velocities are significantly lower in the debris cloud from the orthogonal impact. Test results shown in Figure 10 indicate the debris cloud for shots 84 and 85, having the thicker front plates, had lower velocities than those with the thinner front plates. The calculated velocity values for problem 8.74 agree well with this result also, being shown in Table 7 as definitely lower than the values for a similarly yawed impact on the thinner front plates.

10. CONCLUSIONS

Six conclusions of particular interest from the stainless steel work are:

1. Yaw angle of a cylindrical projectile at impact has a significant effect on shield survivability.
2. Areal density alone may not be enough to adequately model front plate behavior; thickness and material should be considered as separate variables.
3. Stainless steel very possibly is more damaging than can be accounted for by its density alone.
4. The double-layer front plate of shot 83 produced no significant change in survivability.
5. Analytical results and test results are overall in excellent agreement.
6. Hydrocode analysis is a useful tool in design and development of hypervelocity shields.

Yaw Angle. After impact, the debris cloud state, velocity, and spread are important factors in determining the success or failure of the back shield. Front plate thickness and material are two major factors influencing the spread and state of the debris cloud. Referring to Figures 9 and 14, greater thickness corresponds to a more spread out debris cloud. From overall shield results, thicker front plates also affect debris state by more effective projectile breakup. The test results also show that yaw angle is another significant factor affecting the debris produced. Test results indicate that a very low yaw angle corresponds to greater projectile breakup, while a yaw angle close to 45 degrees increases projectile lethality by decreasing breakup. More front plate is necessary to compensate for the effects of yaw angle.

Analytical studies made of the yaw effect, particularly detailed study of the projectile density plots, revealed the phenomena which caused the yawed cylinder to be more lethal than the normally incident cylinder or the sphere of equal mass. This phenomena was the tensile wave breakup and erosion of the projectile material, primarily controlled by the projectile geometry in relation to the initial compression wave formed by the impact with the front plate.

The effect of yaw angle is significant for both survivability and lethality concerns, showing an effect solely due to projectile shape, not mass, velocity, material density, etc.

Areal Density. Indications from the test results covered here indicate that front plate areal density alone is not sufficient to determine projectile breakup, even with yaw angle included. Front plate material and thickness should be considered as separate variables for complete shield design. Material properties of the front plate, such as energy needed to change state and properties when liquified, may be a factor in resolving this completely.

Stainless Steel. The preliminary indications concerning the high level of damage to be expected from stainless steel, perhaps even higher than can be accounted for by density alone, are of further interest. Damage from the stainless steel projectiles was quite high and indicative of incomplete projectile breakup, more so than for shields of similar design ratios used against other projectiles. As suggested above for the front plate, material properties of the projectile relating to liquification, vaporization, and characteristics in these states may be of significance in this area.

Dual Front Plates. For the configuration tested, the two-layer front plate showed no increase in survivability.

Analytical and Experimental Result Agreement. The analytical results produced during this study were generally in excellent agreement with the experimental results. Past experience with the use of the Hull hydrocode indicated this would be the case. At this point, it can be concluded that the Hull code is a valuable tool in hypervelocity shield design, analysis, and testing.

11. RECOMMENDATIONS

Recommendations are given here for further testing and/or analyses needed in several areas.

Weight Reduction. The shield configurations of shots 84 and 85 are 15.6% of the solid aluminum areal density. While this is a very sizeable weight reduction, further reduction down to a 10% level should be achievable. A recommended starting point would be to use the front plate of shot 77 and the disrupter and back plates of shot 84/85. From the spread of damage, referring to Figure 9, and the closeness to success of shot 77, it is highly likely that this configuration would be successful.

Yaw Angle. Since yaw angle is not a controllable variable, its effects could be studied by repeating shots of the same configuration and comparing results. A fuller understanding of yaw effects as a function of yaw angle would be of interest; for example, is 45 degrees really the worst case? Analyses and testing of small yaw angles in particular should be studied. A spinning projectile, for directional stability, would be of interest. Also, the effects of yaw angle as a function of shield configuration are of interest. As previously mentioned, does increasing front plate thickness decrease the yaw effect? Comparison data for spheres of equal mass and equal diameter as any cylindrical projectiles studied would also provide valuable information.

Areal Density. The results of shot 65 and shot 66, along with the results of other researchers, indicate that this area has questions remaining to be answered also. Material selection for a front plate, rather than simply specifying an areal density, needs to be investigated further. Within certain material classes, areal density would likely be the defining variable, but too great a change in material (as from stainless steel to aluminum) appears to have a separate effect apart from areal

density concerns. Recommended tests to begin investigation of this concern would be to test a stainless steel plate of equal thickness as the aluminum plate of shot 66 and to test an aluminum plate of equal areal density as the front shields used for shots 84 and 85.

Projectile Material. The question of what projectile material provides the most lethal impact is of considerable interest. A general idea is that lethality corresponds with projectile density. Projectiles of very high density do have certain disadvantages, such as material availability, toxicity, and machinability. If stainless steel is truly a more lethal projectile than can be accounted for by its density alone, this is of considerable significance in both the survivability and lethality areas. Further testing and analysis would definitely be of interest here. This work should include projectiles of different materials but equal masses, testing/analysis to determine the debris cloud state after impact, and testing/analysis to determine real values for the pressures at impact needed for melting and for vaporization of projectiles.

12. REFERENCES

1. Gehring, J. W., "Theory of Impact on Thin Targets and Shields and Correlation with Experiments," in High Velocity Impact Phenomena, ed. by R. Kinslow (Academic Press, NY, 1970), pp. 105-156.
2. Hart, Bill and Wessel, Frank, "Defensive Shields Demonstration (DSD) Source Book," October 1986, Air Force Contract, pp. 46-47.
3. Maiden, C. L., McMillan, A. R., and Sennett, R. E., "Thin Sheet Impact," NASA CR-295, 1965.
4. Matuska, Daniel A. and Osborn, John I., "Hull Hydrocode Documentation, User's Manual," published 1983, revised 10/87 by Orlando Technology, Inc., Shaliman, FL.
5. Morrison, R. H., "A Preliminary Investigation of Projectile Shape Effects in Hypervelocity Impact of Double-Sheet Structures," NASA TN D-6944, 1972.
6. Piekutowski, Andrew J., "Debris Clouds Generated by Hypervelocity Impact of Cylindrical Projectiles With Thin Aluminum Plates," *International Journal of Impact Engineering* Vol. 5, pp. 509-518, 1987.
7. ORNL Staff, "Final Report of the Technical Progress on the Oak Ridge Fast Track Program April 1986 - September 1987 (U)," published March 1989, prepared under U.S. DOE Contract No. DE-A CO5-84OR21400.

8. Smith, J. E., "Experimental Methods," ORNL TM _____, in press.
9. Swift, H. F., "Hypervelocity Impact Mechanics," in Impact Dynamics, ed. by J. A. Zukas, T. Nicholas, H. F. Swift, L. B. Greszczuk, and D. R. Curan (John Wiley, NY, 1982), pp. 215-240.
10. Swift, H. F. and Hopkins, A. K., J. Spacecraft 7, 1970, pp. 73-77.

INTERNAL DISTRIBUTION

1. D. E. Bartine
2. E. D. Brewer
3. D. W. Burton
4. J. M. Corum
5. E. B. Harris
6. W. R. Hendrich
7. R. L. Huddleston
8. D. T. Ingersoll
9. J. E. Jones Jr.
10. F. C. Maienschein
11. R. T. Santoro
12. J. E. Smith
13. D. G. Thomas
14. ORNL Patent Office
15. Central Research Library
16. Document Reference Section
17. Laboratory Records
18. Laboratory Records (RC)

EXTERNAL DISTRIBUTION

19. Dr. Charles Aeby, AFWL/NTC, Air Force Weapons Laboratory, Kirtland Air Force Base, New Mexico 87117-6008
20. Dr. M. Alme, Computer Sciences Corporation, 2100 Air Park Road SE, Albuquerque, New Mexico 87106
21. Lt. Dale Atkinson, AFWL/NTCA, Air Force Weapons Laboratory, Kirtland Air Force Base, New Mexico 87117-6008
22. Mr. L. Bariess, Martin Marietta Denver Aerospace, P.O. Box 179, Denver, Colorado 80201
23. Bob Becker, U.S. Army Strategic Defense Command, 106 Wynn Drive, SLKT, Huntsville, Alabama 35805
24. Mr. B. Belason, AVCO Specialty Materials, 2 Industrial Way, Lowell, Massachusetts 01851
25. Dr. C. Bersch, Institute for Defense Analysis, 1801 N. Beauregard Street, Alexandria, Virginia 22311
26. R. L. Bjork, PACTECH, P.O. Box 148, Del Mar, California 92014
27. Stan Brockway, Kaman Sciences Corporation, 600 Boulevard South, Huntsville, Alabama 35805
28. Carl Chambers, CSSD-H-LL, U.S. Army Strategic Defense Command, 106 Wynn Drive, Huntsville, Alabama 35805
29. CMDR J. C. Connell, Defense Nuclear Agency, 6801 Telegraph Road, Alexandria, Virginia 22310

30. W. E. Cooper, IN-I, U.S. Army Strategic Defense Command, 106 Wynn Drive, Huntsville, Alabama 35805
31. Dr. B. Cour-Palais, NASA Johnson Space Center, Houston, Texas 77058
32. Jeanne Crews, NASA Johnson Space Center, SN-31, Houston, Texas 77058
33. DETIR, Kaman Sciences Corporation - TEMPO Division, 2560 Huntington Avenue, Suite 500, Alexandria, Virginia 22303-1490
34. DETIR, Kaman Sciences Corporation - TEMPO Division, 816 State Street, P.O. Drawer QQ, Santa Barbara, California 93102-1479
35. James Eamon, Kaman Sciences Corporation, 1500 Garden of the Gods Road, Colorado Springs, Colorado 80933
36. Tosh Fujita, Jet Propulsion Laboratory, 4800 Oak Grove Drive, Pasadena, California 91109
37. Dr. W. Isbell, General Research Corporation, P.O. Box 30400, Santa Barbara, California 93105
38. Richard Jackson, Kaman Sciences Corporation, 600 Boulevard South, Huntsville, Alabama 35805
39. Dick Keefee, Kaman Sciences Corporation, 1500 Garden of the Gods Road, Colorado Springs, Colorado 80933
40. George Landwehr, Teledyne Brown Engineering, 300 Sparkman Drive, Huntsville, Alabama 35807
41. John La Ulibarri, Sandia National Laboratory, 1515 Eubank Boulevard SE, P.O. Box 5800, Albuquerque, New Mexico 87185
42. R. J. Lawrence, Div. 9014, Sandia National Laboratory, 1515 Eubank Boulevard SE, P.O. Box 5800, Albuquerque, New Mexico 87185
43. Lt. Col. C. Lee, SD/CNIV, P.O. Box 92960, Los Angeles Air Force Base, Los Angeles, California 90009-2960
44. Dr. Julius Lilly, U. S. Army Strategic Defense Command, 106 Wynn Drive, CSSD-H-LL, Huntsville, Alabama 35805
45. Dr. J. E. Lowder, SPARTA, Inc., 21 Worthen Road, Lexington, Massachusetts 02173
46. Maj. Thomas McDowell, SDIO/T/SL, Pentagon, Washington, D.C. 20301-7100
47. Dr. W. G. Nichols, Computer Sciences Corporation, 2100 Air Park Road SE, Albuquerque, New Mexico 87106

48. Dr. J. J. O'Sullivan, ANSER Corporation, 1215 Jefferson Davis Hwy., Suite 800, Arlington, Virginia 22202
49. Glenn Ormbrek, AFWAL/MLLN, Wright Research and Development Center, Wright-Patterson Air Force Base, Ohio 45433-6533
50. Glenn Pomykall, Lawrence Livermore National Laboratory, P.O. Box 808, Livermore, California 94550
51. George Schmidt, AFWAL/MLPJ, Wright Research and Development Center, Wright-Patterson Air Force Base, Ohio 45433-6533
52. Dr. William P. Schonberg, Mechanical Engineering Department, University of Alabama at Huntsville, Huntsville, Alabama 35899
53. Dr. P. Seckler, SD/CNWK, P.O. Box 92960, Los Angeles Air Force Base, Los Angeles, California 90009-2960
54. William Tedeschi, Sandia National Laboratory, 1515 Eubank Boulevard SE, P.O. Box 5800, Albuquerque, New Mexico 87185
55. John Tipton, HNDED-SY, U.S. Army Engineering Division, P.O. Box 1600, Huntsville, Alabama, 35807-4301
56. Dr. R. Washburn, SPARTA, Inc., 21 Worthen Road, Lexington, Massachusetts 02173
57. A. E. Williams, Naval Research Laboratory, Washington, D.C. 20375
58. Office of Asst. Manager for Energy Research and Development, DOE-ORO, Oak Ridge, TN 37831
- 59-60. Office of Scientific and Technical Information, P.O. Box 62, Oak Ridge, Tennessee 37830